Cite as: A. Z. Wec *et al.*, *Science* 10.1126/science.aag3267 (2016).

A "Trojan horse" bispecific antibody strategy for broad protection against ebolaviruses

Anna Z. Wec,[1]* Elisabeth K. Nyakatura,[2]* Andrew S. Herbert,[3]* Katie A. Howell,[4] Frederick W. Holtsberg,[4] Russell R. Bakken,[3] Eva Mittler,[1] John R. Christin,[5] Sergey Shulenin,[4] Rohit K. Jangra,[1] Sushma Bharrhan,[1] Ana I. Kuehne,[3] Zachary A. Bornholdt,[6] Andrew I. Flyak,[7] Erica Ollmann Saphire,[6,8] James E. Crowe Jr.,[7,9,10]† M. Javad Aman,[4]† John M. Dye,[3]† Jonathan R. Lai,[2]† Kartik Chandran[1]†

[1]Department of Microbiology and Immunology, Albert Einstein College of Medicine, Bronx, NY 10461, USA. [2]Department of Biochemistry, Albert Einstein College of Medicine, Bronx, NY 10461, USA. [3]United States Army Medical Research Institute of Infectious Diseases, Fort Detrick, MD 21702, USA. [4]Integrated Biotherapeutics Inc., Gaithersburg, MD 20878, USA. [5]Department of Cell Biology, Albert Einstein College of Medicine, Bronx, NY 10461, USA. [6]Department of Immunology and Microbial Science, The Scripps Research Institute, La Jolla, CA 10550, USA. [7]Department of Pathology, Microbiology and Immunology, Vanderbilt University, Nashville, TN 37235, USA. [8]The Skaggs Institute for Chemical Biology, The Scripps Research Institute, La Jolla, CA 10550, USA. [9]Department of Pediatrics, Vanderbilt University, Nashville, TN 37232, USA. [10]Vanderbilt Vaccine Center, Vanderbilt University, Nashville, TN 37232, USA.

*These authors made equivalent contributions.

†Corresponding author. E-mail: kartik.chandran@einstein.yu.edu (K.C.); jon.lai@einstein.yu.edu (J.R.L.); john.m.dye1.civ@mail.mil (J.M.D.); javad@integratedbiotherapeutics.com (M.J.A.); james.crowe@vanderbilt.edu (J.E.C.)

There is an urgent need for monoclonal antibody (mAb) therapies that broadly protect against Ebola virus and other filoviruses. The conserved, essential interaction between the filovirus glycoprotein, GP, and its entry receptor Niemann-Pick C1 (NPC1) provides an attractive target for such mAbs, but is shielded by multiple mechanisms, including physical sequestration in late endosomes. Here, we describe a bispecific antibody strategy to target this interaction, in which mAbs specific for NPC1 or the GP receptor-binding site are coupled to a mAb against a conserved, surface-exposed GP epitope. Bispecific antibodies, but not parent mAbs, neutralized all known ebolaviruses by coopting viral particles themselves for endosomal delivery, and conferred post-exposure protection against multiple ebolaviruses in mice. Such 'Trojan horse' bispecific antibodies have potential as broad anti-filovirus immunotherapeutics.

The development of therapeutics targeting Ebola virus (EBOV) and other filoviruses is a global health priority. The success of ZMapp—a cocktail of three monoclonal antibodies (mAbs) targeting the EBOV surface glycoprotein GP—in reversing Ebola virus disease in nonhuman primates (NHPs) has underscored the promise of antiviral immunotherapy (*1*). However, most available mAbs possess a narrow antiviral spectrum, because they recognize variable surface-exposed GP epitopes (*2*). ZMapp protects against EBOV, but not against other filoviruses with known epidemic potential, including the ebolaviruses Bundibugyo virus (BDBV) and Sudan virus (SUDV), and the more divergent marburgviruses. Given the scientific and logistical challenges inherent in developing a separate mAb cocktail for each filovirus, and the need for preparedness against newly emerging or engineered viral variants, broadly protective anti-filovirus immunotherapies are highly desirable. A few mAbs have shown cross-neutralization and protection in rodents, indicating that cross-species protection by a single molecule is possible; however, such antibodies are rare (*3*–*8*).

An unusual feature of cell entry by filoviruses is the proteolytic cleavage of GP in endosomes to reveal 'cryptic' epitopes (*9*, *10*), including the receptor-binding site (RBS) that engages the critical intracellular receptor, Niemann-Pick C1 (NPC1) (fig. S1) (*11*–*18*). Engagement of NPC1's second luminal domain, NPC1-C, by this highly conserved RBS in cleaved GP (GP_{CL}) is required for cell entry and infection by all filoviruses (*11*, *19*–*21*). Consistent with this, MR72, an RBS-specific mAb isolated from a Marburg virus (MARV) disease survivor, blocked GP_{CL}/NPC1 interaction in vitro, and broadly neutralized viruses bearing in vitro-cleaved GP_{CL} (*15*, *22*, *23*). However, MR72 failed to neutralize infection by uncleaved ebolaviruses, likely because it could not gain access to late endosomes, where the GP_{CL} RBS becomes unmasked (*15*). Therefore, the development of broadly protective immunotherapies targeting GP_{CL}/NPC1 interaction is challenged by the endosomal sequestration of this virus/receptor complex.

We envisioned a bispecific antibody (bsAb) engineering strategy to block intracellular GP_{CL}/NPC1 interaction by a 'Trojan horse' mechanism. We reasoned that, by coupling receptor/RBS-targeting mAbs to a delivery mAb directed against a broadly conserved epitope in uncleaved GP, viri-

ons themselves could be coopted to transport bsAbs to the appropriate endosomal compartments (Fig. 1, A and B). To block the filovirus/receptor interaction, we chose mAbs targeting both its viral and host facets: MR72, a human mAb that recognizes the GP_{CL} RBS (above); and mAb-548, a novel murine mAb that engages human NPC1-C. mAb-548 bound with picomolar affinity to an NPC1-C epitope that overlaps the GP_{CL} binding interface, and blocked GP_{CL}/NPC1-C association in vitro at pH 5.5, the presumptive pH of late endosomes (figs. S1 and S2). mAb-548 resembled MR72 in its lack of neutralizing activity against uncleaved viruses (Fig. 2, A and B, and fig. S6), likely because NPC1 is absent from the cell surface (*11*, *24*). To deliver mAb-548 and MR72 to endosomes, we selected the macaque mAb FVM09, which recognizes a conserved linear epitope in the GP glycan cap of all known ebolaviruses (Fig. 1A and fig. S4) (*8*). FVM09 does not neutralize infection, and confers limited in vivo protection against EBOV (*8*).

The heavy (V_H) and light chain (V_L) variable domains of FVM09 were fused to mAb-548 and MR72 using the dual variable domain design strategy (DVD-Ig) (*25*). The DVD-Ig format was chosen as a test case, because it allows bivalent binding of both combining sites, but does not employ long polypeptide linkers that may be susceptible to proteolysis or immunogenic presentation. The FVM09~548 and FVM09~MR72 DVD-Igs could be readily isolated from transiently-transfected HEK293 cells (fig. S3A). Size-exclusion chromatography-multiangle light scattering (SEC-MALS) indicated a monodisperse population of monomers, with some higher aggregate present (fig. S3, B and C). Each DVD-Ig could bind to EBOV GP via the FVM09 'outer' variable domains, with no loss of affinity relative to the parent FVM09 IgG, as determined by biolayer interferometry (BLI; Fig. 1C and table S1). FVM09~548 could recognize human NPC1-C, via its 'inner' variable domains, with a subpicomolar K_D. The MR72 variable domains also retained subnanomolar affinity toward GP_{CL} in the DVD-Ig format. Two-phase binding studies, in which each DVD-Ig was first exposed to EBOV GP, and then to NPC1-C or GP_{CL} (Fig. 1D), indicated that there were no steric restrictions to engagement of both combining sites.

We tested the DVD-Igs for their capacity to neutralize infection in human cells by recombinant vesicular stomatitis viruses bearing EBOV GP (rVSV-EBOV GP) or control non-filovirus glycoproteins derived from VSV and Andes hantavirus (Fig. 2, A and B, and fig. S5) (*26*). Both FVM09~548 and FVM09~MR72 specifically and potently neutralized rVSV-EBOV GP, whereas the parental mAbs FVM09, mAb-548, and MR72 had little or no neutralizing activity. Equimolar mixtures of the 'delivery' IgG FVM09 with each receptor/RBS-targeting IgG (mAb-548 or MR72) also did not neutralize infection (Fig. 2, A and B), indicating that DVD-Ig antiviral activity requires the physical linkage of delivery and receptor/RBS-binding specificities. Overall, the DVD-Ig IC_{50} values were in the nanomolar range, similar to the measured K_D of the FVM09/GP complex, but higher than those of the mAb-548/NPC1-C and MR72/GP_{CL} complexes.

The GP_{CL}/NPC1 interaction is conserved among filoviruses (*11*, *15*, *21*, *27*, *28*), and thus we postulated that the DVD-Igs would exhibit broad neutralizing activity. rVSVs bearing GP proteins from the four other ebolaviruses were sensitive to neutralization by both DVD-Igs, whereas rVSV-MARV GP was resistant (Fig. 2, C, D, and G), consistent with the known specificity of FVM09 toward ebolaviruses (*8*). We next tested the DVD-Igs against authentic EBOV, BDBV, and SUDV (Fig. 2, E and F). Each ebolavirus was neutralized by both receptor- and RBS-targeting DVD-Igs, but not by the individual parent IgGs (Fig. 2G and fig. S6).

The success of antibody therapeutics has fueled the development of a panoply of optimized bsAb architectures, several of which (including the DVD-Ig) are in clinical trials (*29*). To explore the generality of our strategy to other formats, we generated an FVM09*MR72 'asymmetric IgG' using the DuoBody platform (figs. S7 and S8) (*30*). FVM09*MR72 broadly neutralized rVSVs bearing ebolavirus GPs, albeit with reduced potency against SUDV GP, possibly due to its loss of bivalent recognition of GP and/or GP_{CL}. Nonetheless, these results illustrate that endosomal targeting of the ebolavirus/receptor interaction is amenable to other bispecific antibody formats.

Our observation that bsAbs combining two non-neutralizing antibodies could confer potent neutralization implied critical roles for both binding specificities. This hypothesis is supported by three pieces of evidence. First, the activity of the DVD-Igs against rVSV-EBOV GP particles containing two point mutations in the FVM09 epitope was greatly reduced (Fig. 3A and fig. S9). Second, DVD-Igs bearing mAb-548 and MR72 variable domains with mutations that abolish binding (FVM09~548^{Mut}, FVM09~$MR72^{Mut}$) lacked neutralizing activity (Fig. 3B). Third, FVM09~548 could not neutralize rVSV-EBOV GP infection in a cell line bearing supraphysiological levels of NPC1, likely because NPC1 overexpression saturates available mAb-548 combining sites (Fig. 3C). Viral neutralization by FVM09~MR72 was unaffected in NPC1-overexpressing cells, consistent with the higher affinity of the GP_{CL}/MR72 complex (55 p.m.; table S1), relative to the GP_{CL}/NPC1-C complex (150 μM; (*16*)).

We postulated that the bsAbs harness extracellular virions for their delivery to endosomal sites of filovirus/receptor interaction in the context of natural infection. Accordingly, we evaluated the internalization of DVD-Igs and their parent IgGs into cellular endosomes (Fig. 3D and figs. S10 and S11). Each Ab was covalently labeled with the acid-dependent fluorescent probe pHrodo Red, and

exposed to cells, either alone, or following preincubation with fluorescent rVSV-EBOV GP particles (*19*, *26*). Cells were measured for both virus- and Ab-associated fluorescence by flow cytometry. Virus-negative cells displayed little Ab signal, indicating that neither the DVD-Igs nor their parent IgGs could internalize into cells without virions. By contrast, virus-positive cells were strongly positive for the DVD-Igs, but not for the parent mAb-548 and MR72 IgGs. Concordantly, only FVM09 and the DVD-Igs could efficiently colocalize with virions (Fig. 3E and fig. S12) or EBOV virus-like particles (fig. S13) in $NPC1^+$ late endosomes, where viral membrane fusion takes place (*19*, *31*). These results, together with the capacity of FVM09 to bind EBOV GP with high affinity between pH 5.5–7.5 (fig. S14 and table S1), suggest that virion/bsAb complexes remain associated in early endosomes and traffic together to late endosomes, where proteolytic removal of the GP glycan cap dislodges FVM09, and where mAb-548 and MR72 can engage their respective cellular and viral targets. Collectively, our findings support a two-step 'deliver-and-block' mechanism for bsAb neutralization.

Finally, we evaluated the protective efficacy of the DVD-Igs in two murine models of lethal ebolavirus challenge. Because our prior experiments were conducted in human cells, we first tested DVD-Ig neutralization activity in murine NIH/3T3 cells (fig. S15). Whereas FVM09~MR72 retained full activity, FVM09~548 exhibited poor neutralization in murine cells (fig. S15, A and B). This could be readily explained by FVM09~548's reduced binding affinity for the murine NPC1 ortholog (fig. S15C), and consequent reduced capacity to block GP_{CL}/NPC1 interaction (fig. S15E). The discrepancy between binding of mAb-548 to human and mouse NPC1 likely arises from species-dependent amino acid sequence differences in the mAb-548-binding region of NPC1-C (fig. S16). By contrast, this region in human NPC1-C is identical to those of rhesus macaques and crab-eating (cynomolgus) macaques (fig. S16), which provide the two NHP models of filovirus challenge currently in use. mAb-548 bound strongly to, and inhibited GP_{CL} interaction with, an NHP NPC1 ortholog derived from the mantled guereza, which also shares an identical mAb-548-binding region (fig. S15, D and F). Therefore, while host species-specific differences in NPC1 binding may affect FVM09~548's efficacy in rodents, they are unlikely to do so in NHPs and humans.

Both DVD-Igs were tested for their capacity to protect BALB/c mice when administered two days after a lethal challenge with mouse-adapted EBOV (Fig. 4A) (*32*). FVM09~MR72 afforded a high level of survival (70%) relative to the untreated group, whereas no significant survival was recorded for FVM09~548 and parent IgG mixtures. We also evaluated the DVD-Igs for post-exposure protection against a lethal human SUDV isolate in the immunocompromised Type 1 IFNα/β $R^{-/-}$ mouse model (Fig. 4B) (*7*, *33*). FVM09~MR72 was fully protective, and FVM09~548 provided partial protection, relative to the untreated group. The limited in vivo efficacy of FVM09~548 was consistent with its reduced capacity to inhibit GP_{CL}/murine NPC1 interaction (fig. S15). These findings provide evidence that a bsAb targeting the critical intracellular virus/receptor interaction can confer broad protection against lethal ebolavirus challenge, even under stringent conditions of post-exposure treatment.

Recent antibody discovery efforts have demonstrated the existence of conserved GP surface epitopes that can elicit broadly reactive mAbs with cross-protective potential (*3–7*, *34*). Herein, we describe a complementary strategy to generate broadly protective Abs that target highly conserved epitopes at the intracellular filovirus/receptor interface, which are normally shielded from GP-specific mAbs. Because the 'cryptic epitope'-targeting components of the bsAbs engineered in this study block endosomal receptor binding by all known filoviruses (*15*) (this study), next-generation molecules combining them with appropriate delivery mAbs of viral or cellular origin may afford coverage against all filoviruses, including newly emerging and engineered variants. This Trojan horse bispecific antibody approach may also find utility against other viral pathogens known to use intracellular receptors (e.g., Lassa virus (*35*)), or more generally, to target entry-related virus structural rearrangements that occur only in the endo/lysosomal pathway.

References and Notes

1. X. Qiu, G. Wong, J. Audet, A. Bello, L. Fernando, J. B. Alimonti, H. Fausther-Bovendo, H. Wei, J. Aviles, E. Hiatt, A. Johnson, J. Morton, K. Swope, O. Bohorov, N. Bohorova, C. Goodman, D. Kim, M. H. Pauly, J. Velasco, J. Pettitt, G. G. Olinger, K. Whaley, B. Xu, J. E. Strong, L. Zeitlin, G. P. Kobinger, Reversion of advanced Ebola virus disease in nonhuman primates with ZMapp. *Nature* **514**, 47–53 (2014). Medline
2. C. D. Murin, M. L. Fusco, Z. A. Bornholdt, X. Qiu, G. G. Olinger, L. Zeitlin, G. P. Kobinger, A. B. Ward, E. O. Saphire, Structures of protective antibodies reveal sites of vulnerability on Ebola virus. *Proc. Natl. Acad. Sci. U.S.A.* **111**, 17182–17187 (2014). Medline doi:10.1073/pnas.1414164111
3. K. A. Howell, X. Qiu, J. M. Brannan, C. Bryan, E. Davidson, F. W. Holtsberg, A. Z. Wec, S. Shulenin, J. E. Biggins, R. Douglas, S. G. Enterlein, H. L. Turner, J. Pallesen, C. D. Murin, S. He, A. Kroeker, H. Vu, A. S. Herbert, M. L. Fusco, E. K. Nyakatura, J. R. Lai, Z. Y. Keck, S. K. Foung, E. O. Saphire, L. Zeitlin, A. B. Ward, K. Chandran, B. J. Doranz, G. P. Kobinger, J. M. Dye, M. J. Aman, Antibody treatment of Ebola and Sudan virus infection via a uniquely exposed epitope within the glycoprotein receptor-binding site. *Cell Rep.* **15**, 1514–1526 (2016). Medline doi:10.1016/j.celrep.2016.04.026
4. A. I. Flyak, X. Shen, C. D. Murin, H. L. Turner, J. A. David, M. L. Fusco, R. Lampley, N. Kose, P. A. Ilinykh, N. Kuzmina, A. Branchizio, H. King, L. Brown, C. Bryan, E. Davidson, B. J. Doranz, J. C. Slaughter, G. Sapparapu, C. Klages, T. G. Ksiazek, E. O. Saphire, A. B. Ward, A. Bukreyev, J. E. Crowe Jr., Cross-reactive and potent neutralizing antibody responses in human survivors of natural ebolavirus infection. *Cell* **164**, 392–405 (2016). Medline doi:10.1016/j.cell.2015.12.022
5. J. C. Frei, E. K. Nyakatura, S. E. Zak, R. R. Bakken, K. Chandran, J. M. Dye, J. R. Lai, Bispecific antibody affords complete post-exposure protection of mice from both Ebola (Zaire) and Sudan viruses. *Sci Rep* **6**, 19193 (2016). Medline

doi:10.1038/srep19193
6. W. Furuyama, A. Marzi, A. Nanbo, E. Haddock, J. Maruyama, H. Miyamoto, M. Igarashi, R. Yoshida, O. Noyori, H. Feldmann, A. Takada, Discovery of an antibody for pan-ebolavirus therapy. *Sci Rep* **6**, 20514 (2016). Medline doi:10.1038/srep20514
7. F. W. Holtsberg, S. Shulenin, H. Vu, K. A. Howell, S. J. Patel, B. Gunn, M. Karim, J. R. Lai, J. C. Frei, E. K. Nyakatura, L. Zeitlin, R. Douglas, M. L. Fusco, J. W. Froude, E. O. Saphire, A. S. Herbert, A. S. Wirchnianski, C. M. Lear-Rooney, G. Alter, J. M. Dye, P. J. Glass, K. L. Warfield, M. J. Aman, Pan-ebolavirus and pan-filovirus mouse monoclonal antibodies: protection against Ebola and Sudan viruses. *J. Virol.* **90**, 266–278 (2016). Medline doi:10.1128/JVI.02171-15
8. Z. Y. Keck, S. G. Enterlein, K. A. Howell, H. Vu, S. Shulenin, K. L. Warfield, J. W. Froude, N. Araghi, R. Douglas, J. Biggins, C. M. Lear-Rooney, A. S. Wirchnianski, P. Lau, Y. Wang, A. S. Herbert, J. M. Dye, P. J. Glass, F. W. Holtsberg, S. K. Foung, M. J. Aman, Macaque monoclonal antibodies targeting novel conserved epitopes within filovirus glycoprotein. *J. Virol.* **90**, 279–291 (2016). Medline doi:10.1128/JVI.02172-15
9. K. Chandran, N. J. Sullivan, U. Felbor, S. P. Whelan, J. M. Cunningham, Endosomal proteolysis of the Ebola virus glycoprotein is necessary for infection. *Science* **308**, 1643–1645 (2005). Medline doi:10.1126/science.1110656
10. K. Schornberg, S. Matsuyama, K. Kabsch, S. Delos, A. Bouton, J. White, Role of endosomal cathepsins in entry mediated by the Ebola virus glycoprotein. *J. Virol.* **80**, 4174–4178 (2006). Medline doi:10.1128/JVI.80.8.4174-4178.2006
11. E. H. Miller, G. Obernosterer, M. Raaben, A. S. Herbert, M. S. Deffieu, A. Krishnan, E. Ndungo, R. G. Sandesara, J. E. Carette, A. I. Kuehne, G. Ruthel, S. R. Pfeffer, J. M. Dye, S. P. Whelan, T. R. Brummelkamp, K. Chandran, Ebola virus entry requires the host-programmed recognition of an intracellular receptor. *EMBO J.* **31**, 1947–1960 (2012). Medline doi:10.1038/emboj.2012.53
12. J. E. Carette, M. Raaben, A. C. Wong, A. S. Herbert, G. Obernosterer, N. Mulherkar, A. I. Kuehne, P. J. Kranzusch, A. M. Griffin, G. Ruthel, P. Dal Cin, J. M. Dye, S. P. Whelan, K. Chandran, T. R. Brummelkamp, Ebola virus entry requires the cholesterol transporter Niemann-Pick C1. *Nature* **477**, 340–343 (2011). Medline doi:10.1038/nature10348
13. M. Côté, J. Misasi, T. Ren, A. Bruchez, K. Lee, C. M. Filone, L. Hensley, Q. Li, D. Ory, K. Chandran, J. Cunningham, Small molecule inhibitors reveal Niemann-Pick C1 is essential for Ebola virus infection. *Nature* **477**, 344–348 (2011). Medline doi:10.1038/nature10380
14. A. S. Herbert, C. Davidson, A. I. Kuehne, R. Bakken, S. Z. Braigen, K. E. Gunn, S. P. Whelan, T. R. Brummelkamp, N. A. Twenhafel, K. Chandran, S. U. Walkley, J. M. Dye, Niemann-pick C1 is essential for ebolavirus replication and pathogenesis in vivo. *MBio* **6**, e00565-e15 (2015). Medline doi:10.1128/mBio.00565-15
15. Z. A. Bornholdt, E. Ndungo, M. L. Fusco, S. Bale, A. I. Flyak, J. E. Crowe Jr., K. Chandran, E. O. Saphire, Host-primed Ebola virus GP exposes a hydrophobic NPC1 receptor-binding pocket, revealing a target for broadly neutralizing antibodies. *MBio* **7**, e02154-e15 (2016). Medline
16. H. Wang, Y. Shi, J. Song, J. Qi, G. Lu, J. Yan, G. F. Gao, Ebola viral glycoprotein bound to its endosomal receptor Niemann-Pick C1. *Cell* **164**, 258–268 (2016). Medline doi:10.1016/j.cell.2015.12.044
17. M. A. Brindley, L. Hughes, A. Ruiz, P. B. McCray Jr., A. Sanchez, D. A. Sanders, W. Maury, Ebola virus glycoprotein 1: Identification of residues important for binding and postbinding events. *J. Virol.* **81**, 7702–7709 (2007). Medline doi:10.1128/JVI.02433-06
18. B. Manicassamy, J. Wang, H. Jiang, L. Rong, Comprehensive analysis of Ebola virus GP1 in viral entry. *J. Virol.* **79**, 4793–4805 (2005). Medline doi:10.1128/JVI.79.8.4793-4805.2005
19. J. S. Spence, T. B. Krause, E. Mittler, R. K. Jangra, K. Chandran, Direct visualization of Ebola virus fusion triggering in the endocytic pathway. *MBio* **7**, e01857-e15 (2016). Medline doi:10.1128/mBio.01857-15
20. M. J. Aman, Chasing Ebola through the endosomal labyrinth. *MBio* **7**, e00346-e16 (2016). Medline doi:10.1128/mBio.00346-16
21. M. Ng, E. Ndungo, R. K. Jangra, Y. Cai, E. Postnikova, S. R. Radoshitzky, J. M. Dye, E. Ramírez de Arellano, A. Negredo, G. Palacios, J. H. Kuhn, K. Chandran, Cell entry by a novel European filovirus requires host endosomal cysteine proteases and Niemann-Pick C1. *Virology* **468-470**, 637–646 (2014). Medline doi:10.1016/j.virol.2014.08.019
22. T. Hashiguchi, M. L. Fusco, Z. A. Bornholdt, J. E. Lee, A. I. Flyak, R. Matsuoka, D. Kohda, Y. Yanagi, M. Hammel, J. E. Crowe Jr., E. O. Saphire, Structural basis for Marburg virus neutralization by a cross-reactive human antibody. *Cell* **160**, 904–912 (2015). Medline doi:10.1016/j.cell.2015.01.041
23. A. I. Flyak, P. A. Ilinykh, C. D. Murin, T. Garron, X. Shen, M. L. Fusco, T. Hashiguchi, Z. A. Bornholdt, J. C. Slaughter, G. Sapparapu, C. Klages, T. G. Ksiazek, A. B. Ward, E. O. Saphire, A. Bukreyev, J. E. Crowe Jr., Mechanism of human antibody-mediated neutralization of Marburg virus. *Cell* **160**, 893–903 (2015). Medline doi:10.1016/j.cell.2015.01.031
24. J. P. Davies, Y. A. Ioannou, Topological analysis of Niemann-Pick C1 protein reveals that the membrane orientation of the putative sterol-sensing domain is identical to those of 3-hydroxy-3-methylglutaryl-CoA reductase and sterol regulatory element binding protein cleavage-activating protein. *J. Biol. Chem.* **275**, 24367–24374 (2000). Medline doi:10.1074/jbc.M002184200
25. C. Wu, H. Ying, C. Grinnell, S. Bryant, R. Miller, A. Clabbers, S. Bose, D. McCarthy, R. R. Zhu, L. Santora, R. Davis-Taber, Y. Kunes, E. Fung, A. Schwartz, P. Sakorafas, J. Gu, E. Tarcsa, A. Murtaza, T. Ghayur, Simultaneous targeting of multiple disease mediators by a dual-variable-domain immunoglobulin. *Nat. Biotechnol.* **25**, 1290–1297 (2007). Medline doi:10.1038/nbt1345
26. L. M. Kleinfelter, R. K. Jangra, L. T. Jae, A. S. Herbert, E. Mittler, K. M. Stiles, A. S. Wirchnianski, M. Kielian, T. R. Brummelkamp, J. M. Dye, K. Chandran, Haploid genetic screen reveals a profound and direct dependence on cholesterol for hantavirus membrane fusion. *MBio* **6**, e00801-15 (2015). Medline doi:10.1128/mBio.00801-15
27. M. Ng, E. Ndungo, M. E. Kaczmarek, A. S. Herbert, T. Binger, A. I. Kuehne, R. K. Jangra, J. A. Hawkins, R. J. Gifford, R. Biswas, A. Demogines, R. M. James, M. Yu, T. R. Brummelkamp, C. Drosten, L. F. Wang, J. H. Kuhn, M. A. Müller, J. M. Dye, S. L. Sawyer, K. Chandran, Filovirus receptor NPC1 contributes to species-specific patterns of ebolavirus susceptibility in bats. *Elife* **4**, e11785 (2015). Medline doi:10.7554/eLife.11785
28. E. Ndungo, A. S. Herbert, M. Raaben, G. Obernosterer, R. Biswas, E. H. Miller, A. S. Wirchnianski, J. E. Carette, T. R. Brummelkamp, S. P. Whelan, J. M. Dye, K. Chandran, A single residue in Ebola virus receptor NPC1 influences cellular host range in reptiles. *mSphere* **1**, e00007-16 (2016). Medline doi:10.1128/mSphere.00007-16
29. C. Spiess, Q. Zhai, P. J. Carter, Alternative molecular formats and therapeutic applications for bispecific antibodies. *Mol. Immunol.* **67** (2 Pt A), 95–106 (2015). Medline doi:10.1016/j.molimm.2015.01.003
30. A. F. Labrijn, J. I. Meesters, B. E. de Goeij, E. T. van den Bremer, J. Neijssen, M. D. van Kampen, K. Strumane, S. Verploegen, A. Kundu, M. J. Gramer, P. H. van Berkel, J. G. van de Winkel, J. Schuurman, P. W. Parren, Efficient generation of stable bispecific IgG1 by controlled Fab-arm exchange. *Proc. Natl. Acad. Sci. U.S.A.* **110**, 5145–5150 (2013). Medline doi:10.1073/pnas.1220145110
31. J. A. Simmons, R. S. D'Souza, M. Ruas, A. Galione, J. E. Casanova, J. M. White, Ebolavirus glycoprotein directs fusion through NPC1+ endolysosomes. *J. Virol.* **90**, 605–610 (2016). Medline doi:10.1128/JVI.01828-15
32. M. Bray, K. Davis, T. Geisbert, C. Schmaljohn, J. Huggins, A mouse model for evaluation of prophylaxis and therapy of Ebola hemorrhagic fever. *J. Infect. Dis.* **178**, 651–661 (1998). Medline doi:10.1086/515386
33. J. M. Brannan, J. W. Froude, L. I. Prugar, R. R. Bakken, S. E. Zak, S. P. Daye, C. E. Wilhelmsen, J. M. Dye, Interferon α/β receptor-deficient mice as a model for Ebola virus disease. *J. Infect. Dis.* **212** (Suppl 2), S282–S294 (2015). Medline doi:10.1093/infdis/jiv215
34. Z. A. Bornholdt, H. L. Turner, C. D. Murin, W. Li, D. Sok, C. A. Souders, A. E. Piper, A. Goff, J. D. Shamblin, S. E. Wollen, T. R. Sprague, M. L. Fusco, K. B. Pommert, L. A. Cavacini, H. L. Smith, M. Klempner, K. A. Reimann, E. Krauland, T. U. Gerngross, K. D. Wittrup, E. O. Saphire, D. R. Burton, P. J. Glass, A. B. Ward, L. M. Walker, Isolation of potent neutralizing antibodies from a survivor of the 2014 Ebola virus outbreak. *Science* **351**, 1078–1083 (2016). Medline doi:10.1126/science.aad5788
35. L. T. Jae, M. Raaben, A. S. Herbert, A. I. Kuehne, A. S. Wirchnianski, T. K. Soh, S. H. Stubbs, H. Janssen, M. Damme, P. Saftig, S. P. Whelan, J. M. Dye, T. R. Brummelkamp, Lassa virus entry requires a trigger-induced receptor switch. *Science* **344**, 1506–1510 (2014). Medline doi:10.1126/science.1252480
36. H. W. Ai, N. C. Shaner, Z. Cheng, R. Y. Tsien, R. E. Campbell, Exploration of new

chromophore structures leads to the identification of improved blue fluorescent proteins. *Biochemistry* **46**, 5904–5910 (2007). Medline doi:10.1021/bi700199g
37. J. Sroubek, Y. Krishnan, J. Chinai, S. Buhl, M. D. Scharff, T. V. McDonald, The use of Bcl-2 over-expression to stabilize hybridomas specific to the HERG potassium channel. *J. Immunol. Methods* **375**, 215–222 (2012). Medline doi:10.1016/j.jim.2011.10.014
38. J. Ye, N. Ma, T. L. Madden, J. M. Ostell, IgBLAST: An immunoglobulin variable domain sequence analysis tool. *Nucleic Acids Res.* **41** (W1), W34–W40 (2013). Medline doi:10.1093/nar/gkt382
39. Y. Mazor, I. Barnea, I. Keydar, I. Benhar, Antibody internalization studied using a novel IgG binding toxin fusion. *J. Immunol. Methods* **321**, 41–59 (2007). Medline doi:10.1016/j.jim.2007.01.008
40. A. F. Labrijn, J. I. Meesters, P. Priem, R. N. de Jong, E. T. van den Bremer, M. D. van Kampen, A. F. Gerritsen, J. Schuurman, P. W. Parren, Controlled Fab-arm exchange for the generation of stable bispecific IgG1. *Nat. Protoc.* **9**, 2450–2463 (2014). Medline doi:10.1038/nprot.2014.169
41. J. Misasi, K. Chandran, J. Y. Yang, B. Considine, C. M. Filone, M. Côté, N. Sullivan, G. Fabozzi, L. Hensley, J. Cunningham, Filoviruses require endosomal cysteine proteases for entry but exhibit distinct protease preferences. *J. Virol.* **86**, 3284–3292 (2012). Medline doi:10.1128/JVI.06346-11
42. A. C. Wong, R. G. Sandesara, N. Mulherkar, S. P. Whelan, K. Chandran, A forward genetic strategy reveals destabilizing mutations in the ebolavirus glycoprotein that alter its protease dependence during cell entry. *J. Virol.* **84**, 163–175 (2010). Medline doi:10.1128/JVI.01832-09
43. D. H. Schott, D. K. Cureton, S. P. Whelan, C. P. Hunter, An antiviral role for the RNA interference machinery in *Caenorhabditis elegans*. *Proc. Natl. Acad. Sci. U.S.A.* **102**, 18420–18424 (2005). Medline doi:10.1073/pnas.0507123102
44. P. B. Jahrling, T. W. Geisbert, J. B. Geisbert, J. R. Swearengen, M. Bray, N. K. Jaax, J. W. Huggins, J. W. LeDuc, C. J. Peters, Evaluation of immune globulin and recombinant interferon-alpha2b for treatment of experimental Ebola virus infections. *J. Infect. Dis.* **179** (Suppl 1), S224–S234 (1999). Medline doi:10.1086/514310
45. Ebola haemorrhagic fever in Sudan, 1976. Report of a WHO/International Study Team. *Bull. World Health Organ.* **56**, 247–270 (1978). Medline
46. J. S. Towner, T. K. Sealy, M. L. Khristova, C. G. Albariño, S. Conlan, S. A. Reeder, P. L. Quan, W. I. Lipkin, R. Downing, J. W. Tappero, S. Okware, J. Lutwama, B. Bakamutumaho, J. Kayiwa, J. A. Comer, P. E. Rollin, T. G. Ksiazek, S. T. Nichol, Newly discovered ebola virus associated with hemorrhagic fever outbreak in Uganda. *PLOS Pathog.* **4**, e1000212 (2008). Medline doi:10.1371/journal.ppat.1000212
47. T. Maruyama, L. L. Rodriguez, P. B. Jahrling, A. Sanchez, A. S. Khan, S. T. Nichol, C. J. Peters, P. W. Parren, D. R. Burton, Ebola virus can be effectively neutralized by antibody produced in natural human infection. *J. Virol.* **73**, 6024–6030 (1999). Medline
48. K. L. Warfield, C. M. Bosio, B. C. Welcher, E. M. Deal, M. Mohamadzadeh, A. Schmaljohn, M. J. Aman, S. Bavari, Ebola virus-like particles protect from lethal Ebola virus infection. *Proc. Natl. Acad. Sci. U.S.A.* **100**, 15889–15894 (2003). Medline doi:10.1073/pnas.2237038100

Acknowledgments

The data presented in this manuscript are tabulated in the main paper and in the supplementary materials. We thank C. Harold and T. Alkutkar for technical support. We acknowledge M.D. Scharff, S. Buhl, and the Einstein Macromolecular Therapeutics Development Facility for assistance with generation of mAb-548; E. Ndungo for assistance with hybridoma screening and for provision of purified human-Russell's viper NPC1 chimeras; E.L. Snapp and L. Costantini for generating an NPC1-eBFP2 fusion construct; and A.F. Labrijn, P.W.H.I. Parren, and Genmab for the gift of purified b12*MR72 DuoBody. This work is supported by NIH grants U19 AI109762 (Centers for Excellence in Translational Research) to K.C., J.R.L., J.M.D., and E.O.S.; R01 AI088027 to K.C.; and 1R41 AI122403 to J.R.L. and M.J.A.; JSTO-DTRA project CB04088 to J.M.D.; and a DTRA contract (HDTRA1-13-C-0015) to M.J.A. E.K.N. was also supported by a DAAD (Deutscher Akademischer Austauschdienst, German Academic Exchange Service) fellowship. M.J.A. is president of and owns stocks, and F.W.H. and S.S. own stock options, in Integrated Biotherapeutics. M.J.A., F.W.H., K.A.H., and S.S. are named coinventors on a patent application (WO 2015/200522 A2) submitted by Integrated Biotherapeutics, that covers the endosomal targeting of filovirus bispecific antibodies. A.Z.W., E.K.N., J.R.L., and K.C. are named coinventors on a patent application (PCT/US/16/30652) submitted by Albert Einstein College of Medicine that covers the use of mAb-548 and bispecific antibodies incorporating mAb-548. A.I.F. and J.E.C. Jr. are named coinventors on a patent application (PCT/US2016/019644) submitted by Vanderbilt University Medical Center that covers the use of the MR72 antibody and bispecific antibodies incorporating MR72. mAb-548 and bispecific antibodies incorporating it are available from K.C. under a material transfer agreement with Albert Einstein College of Medicine. MR72 antibody and bispecific antibodies incorporating it are available from J.E.C. Jr. under a material transfer agreement with Vanderbilt University Medical Center.

Supplementary Materials

www.sciencemag.org/cgi/content/full/science.aag3267/DC1
Materials and Methods
Figures S1 to S16
Table S1
References (*36*–*48*)

13 June 2016; accepted 25 August 2016
Published online 8 September 2016
10.1126/science.aag3267

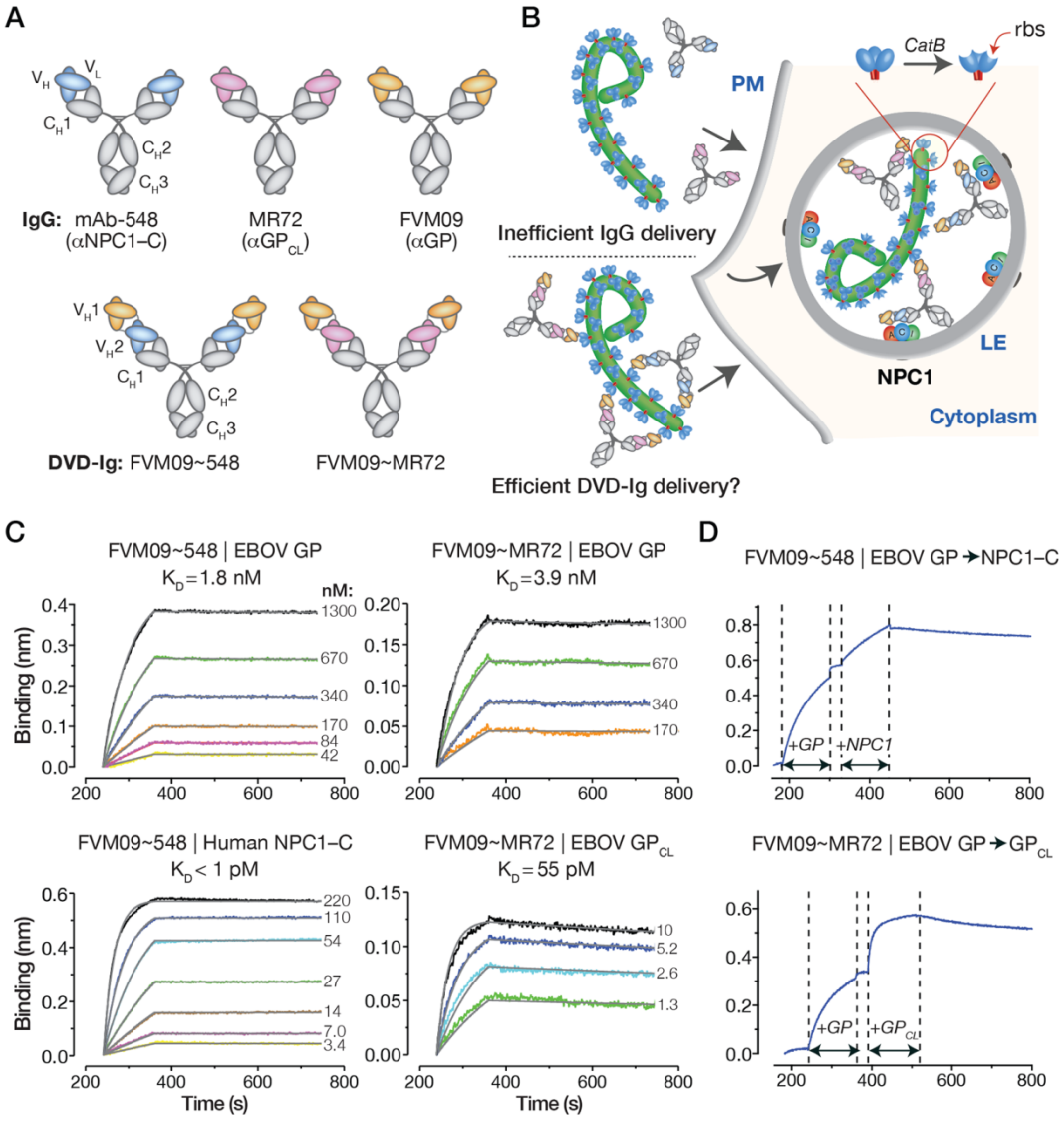

Fig. 1. Dual-variable domain Ig (DVD-Ig) molecules combining extracellular 'delivery' and endosomal receptor/RBS-binding specificities can recognize both of their respective antigens. (**A**) Schematic of mAb-548 and MR72 endosomal receptor/RBS-specific mAbs and FVM09 GP-specific delivery mAb (top row), and DVD-Igs engineered to combine them (bottom row). (**B**) A hypothetical mechanism for delivery of DVD-Igs (bottom), but not parent IgGs (top), to the endosomal sites of GP$_{CL}$-NPC1 interaction. (**C**) Kinetic binding curves for DVD-Ig:antigen interactions were determined by BLI. FVM09~548 (left panel) and FVM09~MR72 (right panel) were loaded onto probes, which were then dipped in analyte solutions (FVM09~548: EBOV GP and human NPC1-C; FVM09~MR72: EBOV GP and GP$_{CL}$). Gray lines show curve fits to a 1:1 binding model. See table S1 for kinetic binding constants. (**D**) Two-phase binding experiments for the DVD-Igs by BLI. Each DVD-Ig-bearing probe was sequentially dipped in analyte solutions containing EBOV GP and then NPC1-C (FVM09~548), or EBOV GP and then GP$_{CL}$ (FVM09~MR72). In panels (C) and (D), representative curves from two independent experiments are shown.

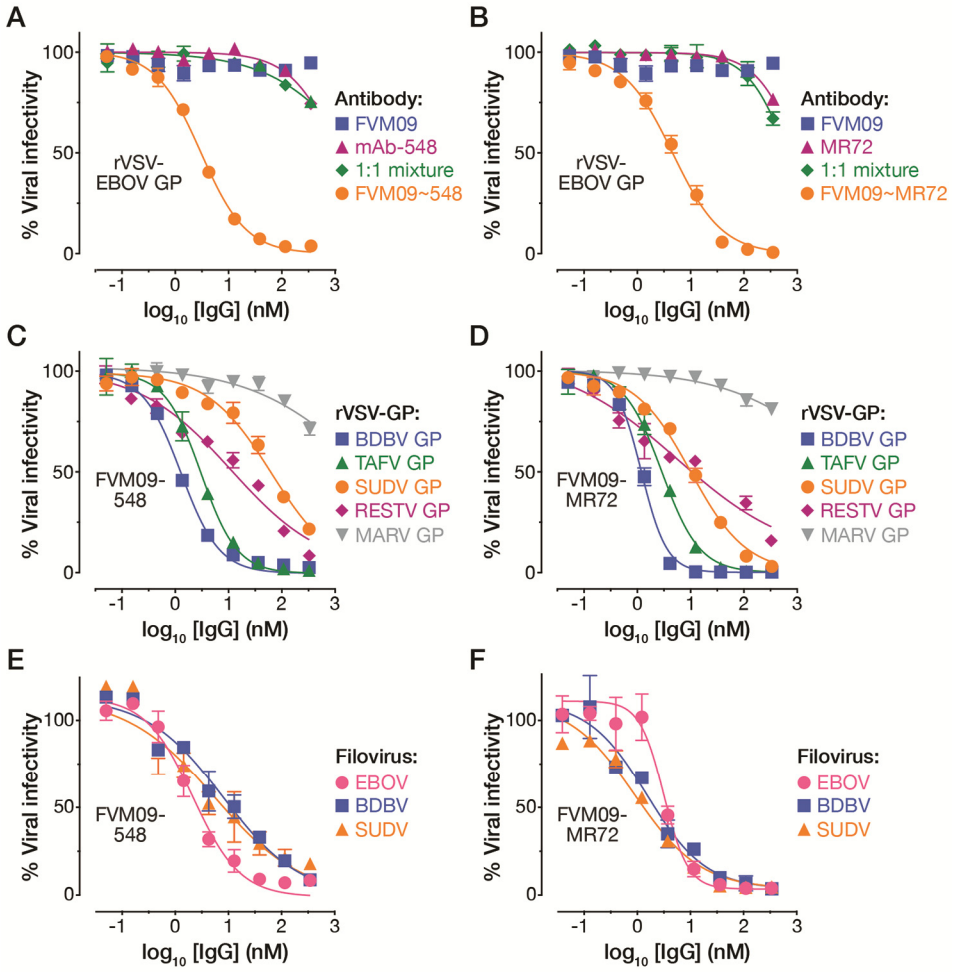

G

Antibody	rVSV-GP IC_{50} (nM) (±95% CI)						Filovirus IC_{50} (nM) (±95% CI)		
	EBOV	BDBV	TAFV	SUDV	RESTV	MARV	EBOV	BDBV	SUDV
FVM09~548	2.9±0.2	1.3±0.1	3.0±0.3	60±10*	12±3*	>350	2.1±0.4	8±3	5±2
FVM09~MR72	4.7±0.5	1.1±0.1	2.9±0.3	10±1	6±1*	>350	3.6±0.7	1.0±0.2	1.8±0.7

Fig. 2. DVD-Igs, but not parent IgGs or their mixtures, possess broad neutralizing activity against ebolaviruses. (**A** to **D**) Neutralization of rVSVs encoding eGFP and bearing filovirus GP proteins in human U2OS osteosarcoma cells. Virions were pre-incubated with increasing concentrations of each parent IgG, DVD-Ig, or equimolar mixtures of parent IgGs (e.g., FVM09+mAb-548) (1:1 mixture), and then exposed to cells for 12–14 hours at 37°C. Infection was measured by automated counting of $eGFP^+$ cells, and normalized to infection obtained in the absence of Ab. TAFV, Taï forest virus; RESTV, Reston virus; MARV, Marburg virus. (**E** to **F**) Neutralization of authentic filoviruses in human U2OS osteosarcoma cells, measured in microneutralization assays. Infected cells were immunostained for viral antigen at 48 hours post-infection, and enumerated by automated fluorescence microscopy. In panels (A) to (F), averages ± SD for 4–6 technical replicates pooled from 2–3 independent experiments are shown. (**G**) Data in panels (A) to (F) were subjected to nonlinear regression analysis to derive Ab concentrations at half-maximal neutralization (IC_{50} ± 95% confidence intervals for nonlinear curve fit). *IC_{50} values derived from curves that did not reach 90% neutralization at the highest concentration tested in the experiments shown.

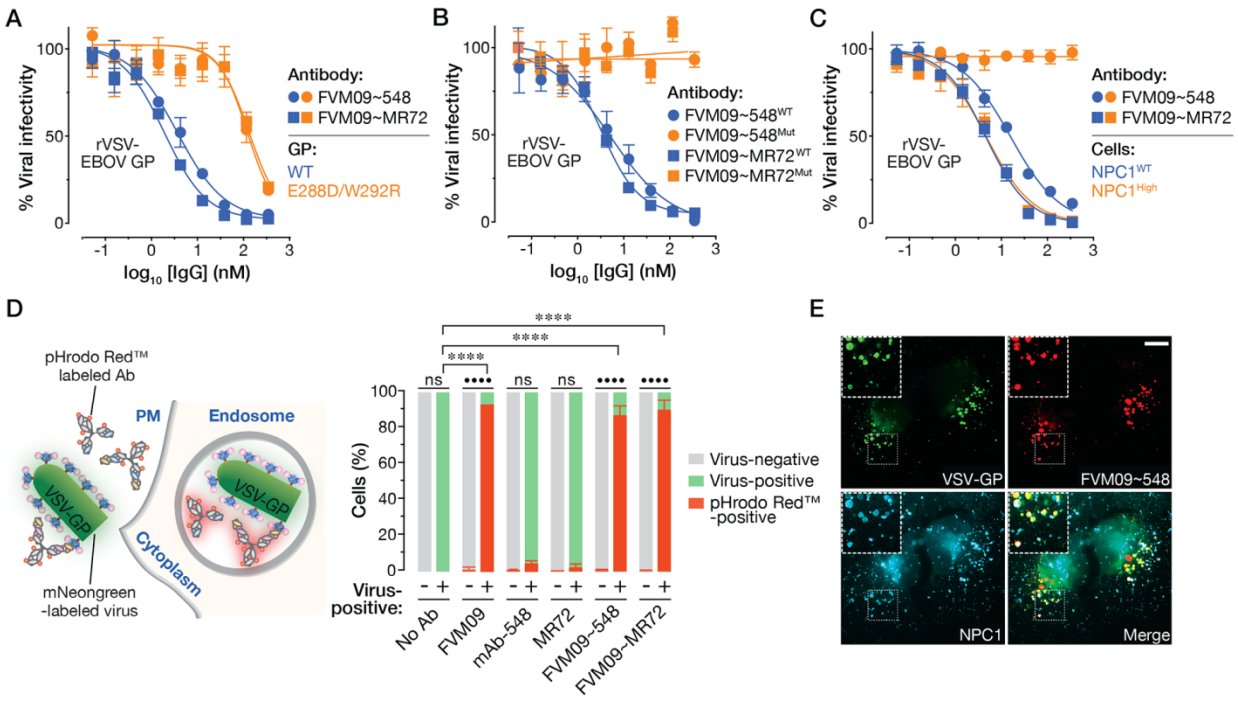

Fig. 3. Roles of delivery and endosomal receptor/RBS-targeting specificities in ebolavirus neutralization by DVD-Igs. (**A**) Neutralizing activity of DVD-Igs against rVSVs bearing WT GP or a GP(E288D/W292R) mutant (see fig. S9). (**B**) Neutralizing activity of mutant DVD-Igs bearing mAb-548 or MR72 combining sites with mutations in the third V_H complementarity determining region (CDR-H3) (FVM09~548^{Mut} and FVM09~MR72^{Mut}, respectively). (**C**) Neutralizing activity of DVD-Igs against rVSV-EBOV GP in U2OS cells bearing endogenous levels of NPC1 (NPC1^{WT}) or ectopically overexpressing NPC1 (NPC1^{High}). In panels (A) to (C), averages ± SD for 6 technical replicates pooled from 2 independent experiments are shown. (**D**) Internalization of labeled Abs into cells in the absence or presence of viral particles. A schematic of the experiment is shown at the left. Parent IgGs and DVD-Igs covalently labeled with the acid-dependent fluorophore pHrodo Red were incubated with rVSV-EBOV GP particles and exposed to cells. Virus$^-$ Ab$^+$ and virus$^+$ Ab$^+$ populations were measured by flow cytometry. Averages ± SD for 4 technical replicates pooled from 2 independent experiments are shown. Group means for %Ab$^+$ cells were compared by two-factor ANOVA (see fig. S11). Šídák's post hoc test was used to compare the capacity of each Ab to internalize into virus$^-$ vs. virus$^+$ cell populations (••••$P < 0.0001$; ns, not significant). Dunnett's post hoc test was used to compare the internalization of each Ab to that of the 'no Ab' control in virus$^+$ cell populations (****$P < 0.0001$; all other Ab vs. no Ab comparisons were not significant). (**E**) Delivery of Abs to NPC1+ endosomes. FVM09~548 was incubated with rVSV-EBOV GP particles and exposed to cells expressing an NPC1-enhanced blue fluorescent protein-2 fusion protein. Viral particles, Ab, and NPC1 were visualized by fluorescence microscopy (also see figs. S12 and S13). Representative images from 2 independent experiments are shown. Scale bar, 20 μm.

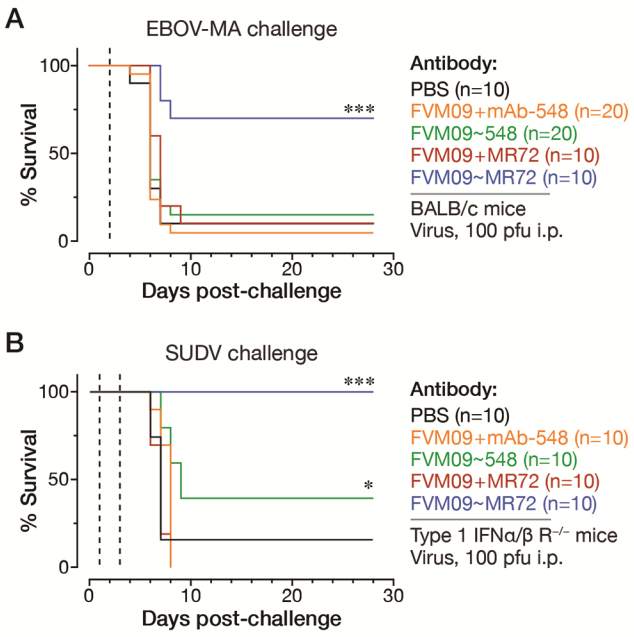

Fig. 4. **FVM09~MR72 affords broad post-exposure protection from lethal ebolavirus challenge.** (**A**) BALB/c mice were challenged with mouse-adapted EBOV (EBOV-MA), and then treated with single doses of parent IgG mixtures (300 µg, ~15 mg/kg), DVD-Igs (400 µg, ~20 mg/kg; adjusted for molecular weight), or vehicle (PBS) at 2 days post-challenge. (**B**) Type 1 IFNα/β $R^{-/-}$ mice were challenged with WT SUDV, and then treated with two doses of parent IgG mixtures (300 µg per dose, ~15 mg/kg), DVD-Igs (400 µg per dose, ~20 mg/kg), or vehicle (PBS) at 1 and 4 days post-challenge. 'n' indicates the number of animals per group. Data from single cohorts are shown. Survival in each group was compared to that in the PBS group by log-rank (Mantel-Cox) test (*$P < 0.05$; ***$P < 0.001$; all other comparisons to the untreated group were not significant).

A "Trojan horse" bispecific antibody strategy for broad protection against ebolaviruses

Anna Z. Wec, Elisabeth K. Nyakatura, Andrew S. Herbert, Katie A. Howell, Frederick W. Holtsberg, Russell R. Bakken, Eva Mittler, John R. Christin, Sergey Shulenin, Rohit K. Jangra, Sushma Bharrhan, Ana I. Kuehne, Zachary A. Bornholdt, Andrew I. Flyak, Erica Ollmann Saphire, James E. Crowe Jr., M. Javad Aman, John M. Dye, Jonathan R. Lai and Kartik Chandran (September 8, 2016)
published online September 8, 2016

Editor's Summary

Science (print ISSN 0036-8075; online ISSN 1095-9203) is published weekly, except the last week in December, by the American Association for the Advancement of Science, 1200 New York Avenue NW, Washington, DC 20005.

www.sciencemag.org/cgi/content/full/science.aag3267/DC1

Supplementary Materials for

A "Trojan horse" bispecific antibody strategy for broad protection against ebolaviruses

Anna Z. Wec, Elisabeth K. Nyakatura, Andrew S. Herbert, Katie A. Howell, Frederick W. Holtsberg, Russell R. Bakken, Eva Mittler, John R. Christin, Sergey Shulenin, Rohit K. Jangra, Sushma Bharrhan, Ana I. Kuehne, Zachary A. Bornholdt, Andrew I. Flyak, Erica Ollmann Saphire, James E. Crowe Jr.,* M. Javad Aman,* John M. Dye,* Jonathan R. Lai,* Kartik Chandran*

Corresponding author. Email: kartik.chandran@einstein.yu.edu (K.C.); jon.lai@einstein.yu.edu (J.R.L.); john.m.dye1.civ@mail.mil (J.MD.); javad@integratedbiotherapeutics.com (M.J.A.); james.crowe@vanderbilt.edu (J.E.C.)

Published 8 September 2016 on *Science* First Release
DOI: 10.1126/science.aag3267

This PDF file includes

Supplementary Materials:

Materials and Methods

Figures S1-S16

Table S1

References

Materials and Methods:

Cell lines. Human U2OS osteosarcoma cells, 293T human embryonic kidney fibroblast cells, and Free-style™-293F suspension-adapted HEK-293 cells were obtained from ATCC. U2OS cells were maintained in modified McCoy's 5A media (Thermo Fisher, Waltham, MA) supplemented with 10% fetal bovine serum (Atlanta Biologicals), 1% GlutaMAX (Thermo Fisher), and 1% penicillin-streptomycin (Thermo Fisher). Vero and 293T cells were maintained in high-glucose Dulbecco's modified Eagle medium (DMEM; Thermo Fisher) supplemented with the above reagents. All adherent cell lines were maintained in a humidified 37˚C, 5% CO_2 incubator. 293-F cells were maintained in GIBCO Free-Style™ 293 expression medium (Thermo Fisher) at 37˚C and 8% CO_2.

A clonal U2OS cell line stably expressing human NPC1 C–terminally tagged with enhanced blue fluorescent protein-2 (eBFP2) (*36*) was generated as follows. Cells were transfected with a plasmid encoding this construct, and transfected cells were selected with geneticin (Thermo Fisher; 400 μg/mL). Single eBFP2-positive cells were isolated by FACS sorting. For further experimentation, we chose a cell clone that expressed NPC1-eBFP2 at a moderate level, and displayed a representative NPC1 distribution in $LAMP1^+$ late endosomal/lysosomal compartments.

Generation of mAb-548. To generate hybridomas secreting human NPC1–C-specific mAbs, 5–6-week old female BALB/c mice were immunized with purified human NPC1–C protein (125 μg; intraperitoneal [i.p.] route) in complete Freund's adjuvant. After 5 weeks and 10 weeks post-immunization, mice were boosted with the same antigen in incomplete Freund's adjuvant. Nine weeks after the second boost, and on the 4^{th} and 3^{rd} days prior to fusion, mice were boosted with NPC1–C in PBS (100 μg). Mice were sacrificed, and spleen cells were isolated and fused to Ag8.653 or NSO-bcl2 myeloma cells as described previously (*37*). Supernatants from growing wells were assayed by ELISA against NPC1–C for IgG binding. Positive colonies were cloned in soft agar, isolated and expanded, and tested as above. One hybridoma, 548, was identified as secreting an IgG2b that strongly recognized human NPC1 in cells by immunofluorescence microscopy, and potently blocked EBOV GP_{CL}:NPC1–C binding at pH 5.5.

5–10 million cells of the mAb-548-secreting hybridoma were harvested, and total cellular RNA was isolated using the RNeasy Mini Kit (Qiagen), according to the manufacturer's instructions. cDNA was prepared using SuperScript® III First-Strand Synthesis System with Mu IgG VH 3′-2 and Mu Igκ VL 3′-1 reverse primers from the Mouse Ig-Primer Set (EMD Millipore, Billerica, MA). Following reverse transcription, the same primer sets were then used in PCR to specifically amplify the variable regions of light- and heavy-chain cDNAs. Reactions yielding the correct band size (~500 bp) were gel-purified and sequenced. Decoded light and heavy chain sequences were submitted for analysis to IgBLAST (*38*). Functional chains were subcloned into pMAZ-IgL and pMAZ-IgH vectors, and the chimeric IgGs were expressed in 293-F cells, as described below.

Cloning of IgGs and DVD-Igs. Synthetic genes encoding IgG variable domains were subcloned into linearized pMAZ-IgH and pMAZ-IgL vectors encoding human IgG1 heavy and light chain constant

domains using BssHII/BsiWI and BssHII/NheI restriction sites, respectively, as described (*39*). To generate DVD-Igs, the outer variable domains of the heavy and light chains were appended N-terminally, using short linkers "ASTKGP" and "TVAAP", respectively, as described (*25*). All insert and junction sequences were confirmed by Sanger sequencing.

Antibody expression and purification. pMAZ-IgH and pMAZ-IgL vectors encoding each antibody were co-transfected into 293-F cells using linear polyethylenimine (Polysciences, Warrington, PA). Cell cultures were incubated at 37 °C and 8% CO_2 for 6 days post-transfection. Cleared cell supernatants were then applied to a Protein A affinity column (~1 mL packed beads per 600 mL culture) (Thermo Scientific). Antibodies were purified using the Gentle Antibody Elution System (Thermo Scientific), according to the manufacturer's instructions, and subsequently exchanged into 150 mM HEPES [pH 7.4], 200 mM NaCl. For some large-scale preparations, cell supernatants were concentrated by tangential flow filtration prior to Ab purification. Endotoxin levels in the purified antibodies were determined by the Limulus amebocyte lysate test according to the manufacturer's instructions (Kinetic-QCL kinetic chromogenic LAL assay; Lonza, Walkersville, MD).

Generation of DuoBody™ molecules by controlled Fab-arm exchange (cFAE). Parental IgG1 antibody molecules containing matching point mutations, K409R and F405L (EU numbering convention), in their CH3 domains were separately expressed from respective pMAZ-IgH and pMAZ-IgL vectors in 293-F cells (see above). cFAE was performed as described (*40*). Briefly, in a total reaction volume of 1 mL, 0.5 mg of each parental IgG1 was mixed with the reducing agent 2-mercaptoetylamine HCL (2-MEA; Sigma Aldrich; 75 mM) in PBS pH 7.4. Samples were mixed on a rotating laboratory mixer for 5 min at ambient temperature and subsequently incubated at 31°C for 5 h. To remove 2-MEA and allow for reformation of disulfide bonds, the samples were transferred to Amicon Ultra-15 centrifugal units (30 KDa MWCO; EMD Millipore) and washed 5 times with phosphate-buffered saline (PBS). The samples were then stored at 4 °C, to allow sufficient time for complete re-oxidation to occur. Fab-arm exchange was detected by matrix-assisted laser desorption/ionization mass spectrometry (MALDI-MS), and analysis of exchange efficiency was carried out by cation exchange chromatography on a MonoS 5/50 GL column (GE Healthcare). Samples were injected in 10 µL into 10 mM sodium phosphate [pH 7.0], and eluted in a linear NaCl gradient (0–100 mM; 20 mL). Elution curves for each antibody species were integrated, and the percentage of the FVM09∗MR72 DuoBody that is distinct from either of the parent IgGs, was calculated as 97%.

Size Exclusion Chromatography/Multi Angled Light Scattering (SEC/MALS). Static light scattering data were collected on a mini Dawn Treos light scattering instrument (Wyatt Technology, Santa Barbara, CA) coupled with analytical gel filtration (column: Sepax SRT SEC-300; particle size 5 µm, pore size 500 Å, 4.6 x 300 mm) and UV detection at 280 nm. All measurements were performed in PBS at room temperature with a flow rate of 0.5 mL/min. Data were analyzed using the ASTRA software package (Wyatt Technology).

Biolayer interferometry (BLI). The OctetRed™ system (ForteBio, Pall LLC) was used to determine the binding properties of IgGs and DVD-Igs. Anti-human Fc capture sensors were used for initial Ab loading. For single-phase binding experiments, global data fitting to a 1:1 binding model was used to estimate values for the k_{on} (association rate constant), k_{off} (dissociation rate constant), and K_D (equilibrium dissociation constant). For double-phase binding experiment, Ab was first immobilized first onto an Fc sensor, and then allowed to equilibrate in a solution containing the first antigen. The sensor was then transferred to a second solution containing the second antigen.

ELISAs. Cell supernatants containing flag-tagged NPC1–C, or purified flag-tagged NPC1–C proteins (*11, 28*), were normalized for ELISA as described previously, by immunoblotting of SDS-

polyacrylamide gels with anti-flag primary antibody (Sigma Aldrich) and anti-mouse Alexa-680 secondary antibody (Thermo Fisher), and quantification on the LI-COR Odyssey Imager (LI-COR Biosciences, Lincoln, NE) (*27*). The GP content of different rVSV-GP particle preparations was normalized by ELISA with a GP-specific polyclonal antiserum (*41*), as described previously (*15*).

NPC1–C:Ab and GP:Ab-binding ELISAs were performed as follows. Pre-titrated amounts of purified NPC1–C or rVSV-GP particles were coated onto high-binding 96-well ELISA plates (Corning, Corning NY). Plates were then blocked with PBS containing 3% bovine serum albumin (PBSA), and probed with increasing concentrations of test Ab. Bound Abs were detected with species-specific anti-IgG Abs conjugated to horseradish peroxidase (Santa Cruz Biotechnology, Dallas, TX) and Ultra-TMB colorimetric substrate (Thermo Fisher).

EBOV GP:NPC1–C capture ELISAs were performed as described previously (*15, 27, 28*). Briefly, ELISA plates were coated with EBOV GP-specific mAb KZ52 (2 μg/mL in PBS), and then blocked with PBSA. Viral particles were cleaved with thermolysin and captured onto the plate. Plates were then incubated with increasing concentrations of NPC1–C, and bound NPC1–C was detected with an anti-flag antibody conjugated to horseradish peroxidase and Ultra-TMB substrate (Thermo Fisher). For Ab inhibition studies, NPC1–C (concentration ≈ binding IC_{50}) was preincubated with increasing concentrations of test Ab at 37˚C for 1 h, and then added to blocked plates coated with rVSV-EBOV GP_{CL}. EC_{50} values with 95% confidence intervals were calculated from binding curves generated by non-linear regression analysis using Prism (GraphPad Software, La Jolla CA). All incubation steps were done at 37˚C for 1 h, or at 4˚C, overnight.

rVSVs, infections, and neutralization dose curves. A recombinant vesicular stomatitis Indiana viruses (rVSV) expressing eGFP in the first position, and EBOV GP in place of VSV G, has been described previously (*26, 42*). Similar rVSVs expressing eGFP and representative GP proteins from BDBV, TAFV, SUDV, and RESTV; and an mNeongreen-phosphoprotein P (mNG-P) fusion protein (*26, 43*) and EBOV GP, were generated as above. rVSV particles containing GP_{CL} were generated by incubating rVSV-GP particles with thermolysin (200 μg/mL) for 1 h at 37˚C, as described. The protease was inactivated by addition of phosphoramidon (Sigma Aldrich; 1 mM), and reaction mixtures were used immediately. Infectivities of rVSVs were measured by automated enumeration of $eGFP^+$ cells (infectious units; IU) using a CellInsight CX5 imager (Thermo Fisher) at 12–14 h post-infection.

For Ab neutralization experiments, pre-titrated amounts of rVSV-GP particles (MOI ≈ 1 IU per cell) were incubated with increasing concentrations of test Ab at room temp for 1 h, prior to addition to cell monolayers in 96-well plates. Viral infectivities were measured as above. Viral neutralization data were subjected to nonlinear regression analysis to extract EC_{50} values (4-parameter, variable slope sigmoidal dose-response equation; GraphPad Prism). Neutralization dose curves shown in Figures 2–3 are representative of multiple additional experiments performed independently, with at least 2–3 different preparations of each antibody.

Authentic filoviruses and infections. The authentic filoviruses Ebola virus/H.sapiens-tc/COD/1995/Kikwit-9510621 (EBOV/Kik-9510621; 'EBOV-Zaire 1995') (*44*), mouse-adapted EBOV (EBOV-MA; derived from Mayinga variant) (*32*), Sudan virus/H. sapiens-gp-tc/SDN/1976/Boniface-USAMRIID111808 (SUDV/Bon-USAMRIID111808; 'SUDV-Boniface 1976') (*45*), and Bundibugyo virus/H. sapiens-tc/UGA/2007/Bundibugyo-200706291 (*46*) were used in this study. Antibodies were diluted to indicated concentrations in culture media and incubated with EBOV, SUDV, or BDBV for 1 h. U2OS cells were exposed to antibody/virus inoculum at an MOI of 0.2 (EBOV, BDBV) or 0.5 (SUDV) plaque-forming unit (PFU)/cell for 1 h. Antibody/virus inoculum was then removed and fresh culture media was added. At 48 h post-infection, cells were fixed with formalin, and blocked with 1% bovine serum albumin. EBOV-, SUDV-, or BDBV-infected cells and uninfected controls were incubat-

ed with EBOV GP-specific mAb KZ52 (*47*), SUDV GP-specific mAb 3C10 (USAMRIID), or ebolavirus GP-specific mAb ADI-15742 (*34*). Cells were washed with PBS prior to incubation with either goat anti-mouse IgG or goat anti-human IgG conjugated to Alexa 488. Cells were counterstained with Hoechst stain (Invitrogen), washed with PBS and stored at 4°C. Infected cells were quantitated by fluorescence microscopy and automated image analysis. Images were acquired at 20 fields/well with a 20× objective lens on an Operetta high content device (Perkin Elmer, Waltham, MA). Operetta images were analyzed with a customized scheme built from image analysis functions available in Harmony software.

Virus-like particles. EBOV virus-like particles (VLPs) were generated essentially as described (*48*), by co-transfection of 293T cells with EBOV GP and EBOV matrix protein VP40, and concentrated by ultracentrifugation through a 20–60% (wt/vol) sucrose gradient. Aliquots of VLPs were bath-sonicated briefly, prior to addition to cells.

Phrodo Red™-labeling and flow cytometry. To analyze Ab internalization into cells during infection, DVD-Igs and parental IgGs were first labeled with the acid-sensitive fluorophore, Phrodo Red. Abs were exchanged into PBS, and covalently conjugated to pHrodo Red succinimidyl ester (Thermo Fisher), according to the manufacturer's instructions. Labeling reactions contained a 5-fold molar excess of dye over Ab. Following conjugation, excess unconjugated dye was removed using PD-10 desalting columns (GE healthcare, Wauwatosa, WI), and Ab-pHrodo Red conjugates were exchanged into PBS and concentrated with Amicon Ultra filters (EMD Millipore; membrane NMWL 50 kDa). Protein concentration and degree of labeling were determined according to the manufacturer's instructions.

Labeled IgGs and DVD-Igs (final concentration, 29 nM) were incubated for 1 h at room temp, in the absence or presence of rVSV(mNG-P)-EBOV GP particles (3.4×10^4 infectious units per well). Virus, Ab, and virus-Ab mixtures were then added to wells of a pre-chilled 6-well plate containing confluent monolayers of U2OS cells. Viral particles were 'spinoculated' onto cells by centrifugation of the plates at 1,500 ×g in a swing-out rotor. Unbound virus was removed by washing with cold PBS, fresh culture media was added, and cells were allowed to internalize viral particles and/or Abs at 37˚C. After 30 min, cells were returned to ice, washed with cold PBS, and then harvested using cold trypsin-EDTA (Thermo Fisher). Harvested cells were kept on ice, filtered through mesh caps at 4˚C, and analyzed for virus (mNG-P) and Ab (pHrodo Red) fluorescence on a BD LSRII flow cytometer, using the gating scheme described in fig. S11.

Immunofluorescence microscopy and co-immunostaining. To investigate transport of parent IgGs and DVD-Igs into target cells, pre-titrated amounts of rVSV(mNG-P)-EBOV GP particles or EBOV VLPs were preincubated with Abs (100 nM) for 1 h at room temp. VSV-antibody complexes were diluted into imaging buffer (20 mM HEPES[pH 7.4], 140 mM NaCl, 2.5 mM KCl, 1.8 mM $CaCl_2$, 1 mM $MgCl_2$, 5 mM glucose, 2% FBS), and spinoculated onto pre-chilled U2OS cells on coverslips stably expressing NPC1-EBFP2 as described above. Unbound virus was removed by washing with cold PBS. Cells were then placed in warm imaging buffer, and allowed to internalize viral particles and/or Abs for 45 min–1 h at 37°C. Cells were fixed with 3.7% paraformaldehyde and permeabilized with PBS/0.1% Triton X-100. NPC1 was detected with primary mouse or rabbit anti-BFP Abs and secondary anti-mouse or anti-rabbit antibody-Alexa 405 fluorophore conjugates, respectively (Thermo Scientific). VP40 was detected with a primary anti-VP40 mAb and a secondary anti-mouse antibody-Alexa 488 fluorophore conjugate. Internalized Abs were visualized by staining with a secondary anti-human Alexa 555 antibody-fluorophore conjugate. Imaging was performed on an Axio Observer Z1 widefield fluorescence microscope (Zeiss Inc., Thornwood, NY) equipped with a 63×/1.4 numerical aperture oil immersion objective. Images were captured with a ORCA-Flash4.0 LT digital CMOS camera (Hamamatsu Photonics, Bridgewater, NJ), and processed in Photoshop (Adobe Systems, San Jose, CA).

Animal challenge studies. Female BALB/c mice (Jackson Labs, Bar Harbor, ME) were challenged via the intraperitoneal (i.p.) route with EBOV-MA (100 PFU; ~3,000 LD_{50}). Mice were treated i.p. 2 days post-challenge with PBS vehicle, 300 μg (≈15 mg/kg) of parent IgG mixtures (187.5 μg each), or 400 μg DVD-Ig (≈20 mg/kg; dose adjusted to account for the higher molecular weight of DVD-Igs). Mice were observed daily for clinical signs of disease and lethality. Daily observations were increased to a minimum of twice daily while mice were exhibiting signs of disease. Moribund mice were humanely euthanized on the basis of IACUC- approved criteria.

6–8 week old male and female Type 1 IFN α/β receptor knockout mice (Type 1 IFNα/β R−/−) (Jackson Labs) were challenged with WT SUDV (1000 PFU i.p.). Mice were treated i.p. 1 and 4 days post-challenge with PBS vehicle, 300 μg (≈15 mg/kg) of parent IgG mixtures per dose (150 μg each) or 400 μg (≈20 mg/kg) DVD-Ig per dose, and monitored as above.

Animal welfare statement. Generation of murine hybridomas and murine challenge studies were conducted under IACUC-approved protocols in compliance with the Animal Welfare Act, PHS Policy, and other applicable federal statutes and regulations relating to animals and experiments involving animals. The facilities where this research was conducted (Albert Einstein College of Medicine and USAMRIID) are accredited by the Association for Assessment and Accreditation of Laboratory Animal Care, International (AAALAC) and adhere to principles stated in the Guide for the Care and Use of Laboratory Animals, National Research Council, 2011.

Statistical analysis. Dose-response neutralization curves were fit to a logistic equation by nonlinear regression analysis. 95% confidence intervals (95% CI) for the extracted IC_{50} parameter were estimated under the assumption of normality. Statistical comparison of means among multiple independent groups in Fig. 3D was carried out by two-factor analysis of variance (ANOVA) with Šídák's and Dunnett's *post hoc* tests to correct for multiple comparisons (see fig. S11). Analysis of survival curves in Fig. 4 was performed with the Mantel-Cox (log-rank) test. Testing level (alpha) was 0.05 for all statistical tests. All analyses were carried out in GraphPad Prism.

figure S1

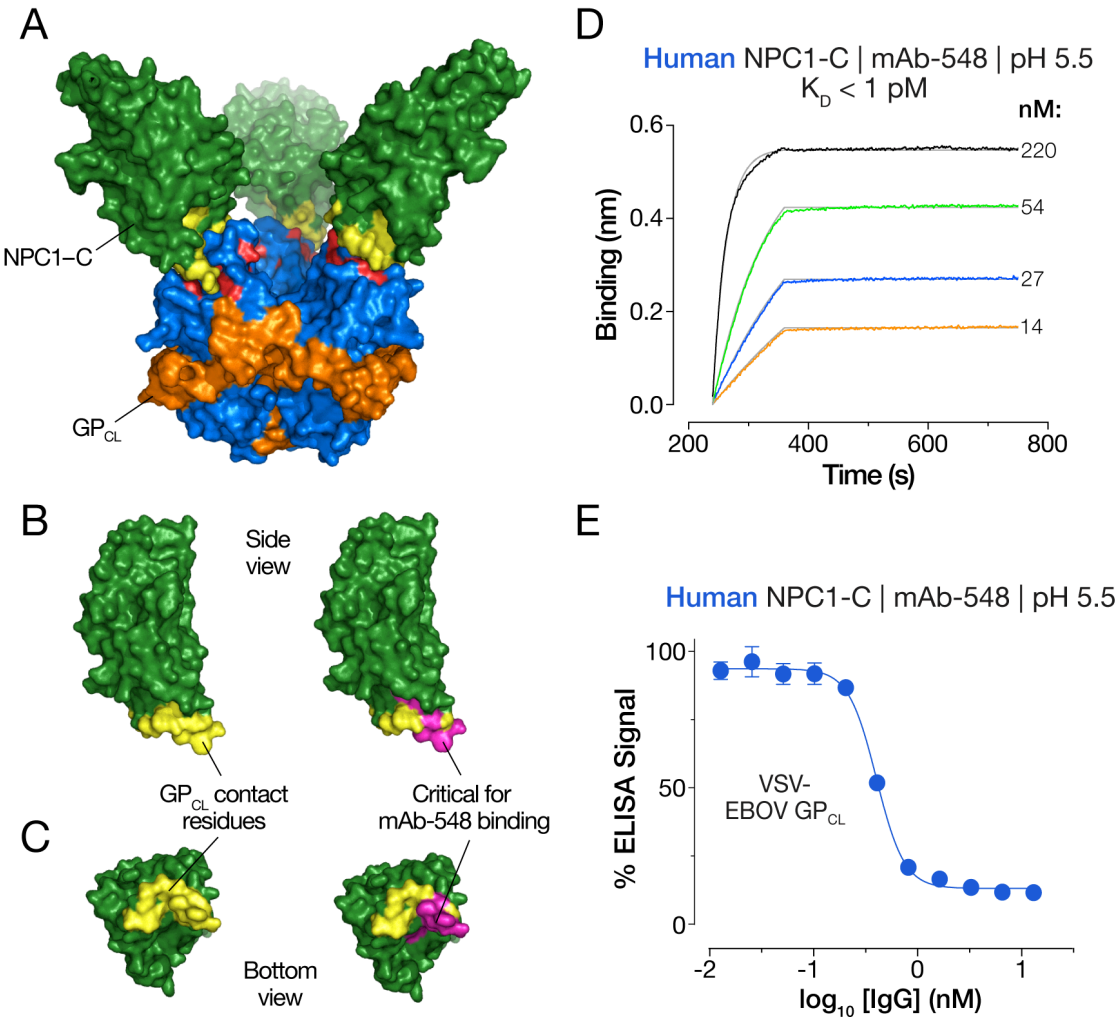

Figure S1. mAb-548 targets the GP_{CL}-binding site in NPC1 domain C (NPC1–C), and blocks GP_{CL}:NPC1–C binding *in vitro*. (A) Surface-shaded representation of the X-ray crystal structure of an EBOV GP_{CL}:NPC1–C complex (PDB ID: 5F1B) (*16*). Green, NPC1–C; blue, GP1; orange, GP2; red, GP_{CL} receptor-binding site (RBS) residues; yellow, GP_{CL} contact residues in NPC1–C. (B–C) Structure of NPC1–C. GP_{CL} contact residues (yellow) and residues critical for mAb-548 binding (pink) are highlighted. (D) Kinetic binding curves for mAb-548:human NPC1–C interaction were determined by biolayer interferometry (BLI). mAb-548 was loaded onto the probe, which was then dipped in solutions containing increasing concentrations of NPC1–C (nM; indicated for each curve). (E) Dose-dependent inhibition of rVSV-EBOV GP_{CL}:NPC1–C binding by mAb-548 in a competition ELISA. Averages ± SD for 6 technical replicates pooled from 2 independent experiments are shown.

figure S2

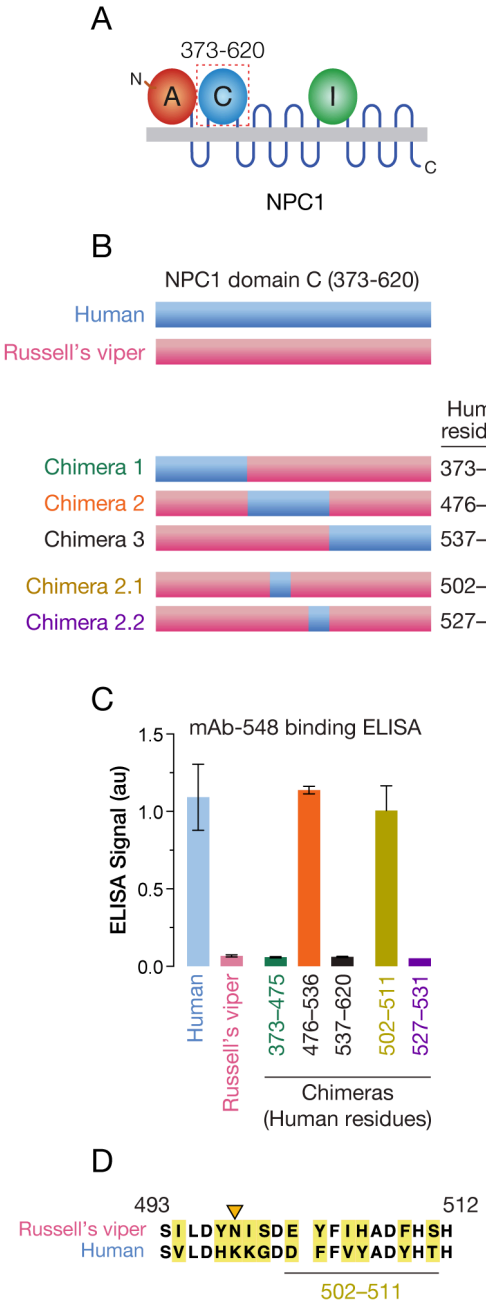

Figure S2. Mapping the mAb-548 binding site in human NPC1–C. (A) Cartoon line diagram of human NPC1 with the second luminal domain, domain C, highlighted. (B–C) Using a species-specific difference in mAb-548 recognition to map its binding site in human NPC1–C:mAb-548 recognizes human NPC1–C, but not NPC1–C derived from the Russell's viper (*Daboia russellii*) in an ELISA (C). A panel of chimeras between human and Russell's viper NPC1–C, in which human sequences were introduced into the Russell's viper background (*28*) (B) were tested for mAb-548 binding by ELISA (C). This gain-of-function genetic analysis demonstrated that NPC1 residues 502–511 (human numbering) contain residues critical for mAb-548 recognition (D). In panel C, averages ± SD for 3 technical replicates from a representative experiment are shown. Two independent experiments were performed. In panel D, amino acid sequence differences are shown in yellow. The inverted orange triangle indicates an N–linked glycosylation site present in Russell's viper NPC1–C, but not in human NPC1–C.

figure S3

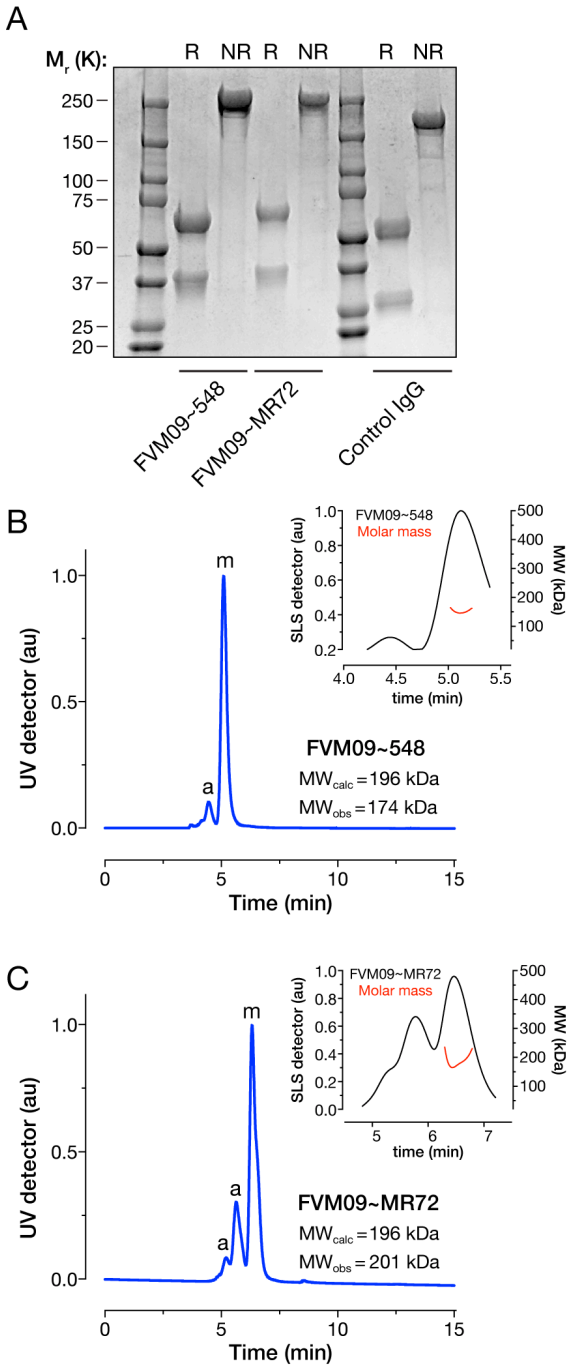

Figure S3. Biochemical characterization of DVD-Igs. (A) FVM09~548 and FVM09~MR72 were resolved on SDS-polyacrylamide gels under reducing (R) and nonreducing (NR) conditions, and proteins were visualized by staining with Coomassie Brilliant Blue. A control IgG is shown for comparison. The DVD-Igs migrated as a disulfide-bonded complex (relative molecular weight, M_r ≈200K). (B–C) Size exclusion chromatography-multiangle light scattering (SEC-MALS) analysis of FVM09~548 (B) and FVM09~MR72 (C). Absorbance (arbitrary units; au) was monitored at 280 nm. m, monomer peak. a, aggregate peak. Calculated (MW_{calc}) and observed (MW_{obs}) molecular weight estimates from MALS are shown in inset. In panels B–C, representative traces from two independent experiments are shown.

figure S4

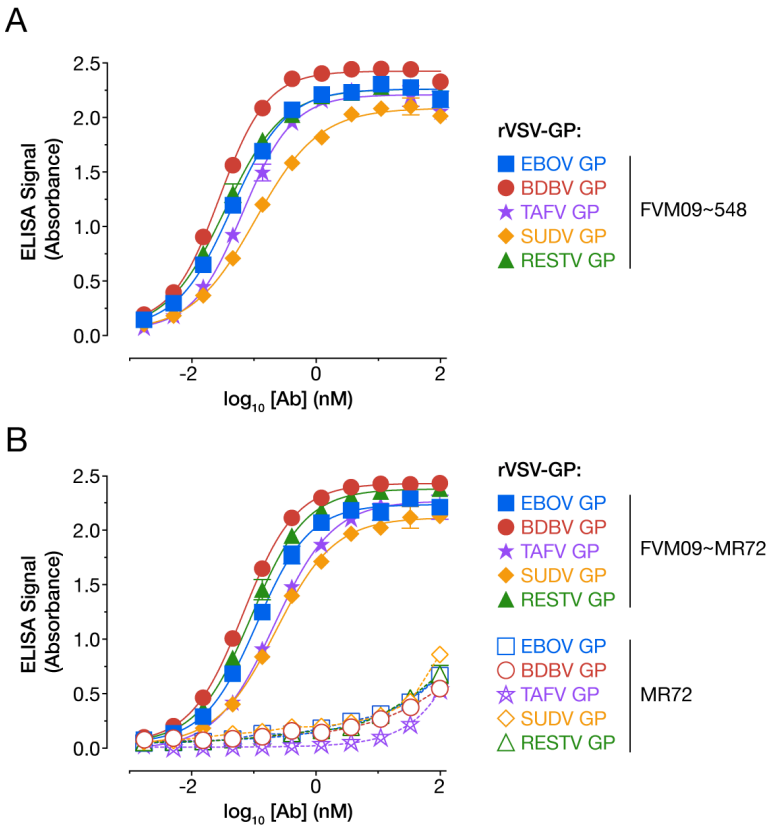

Figure S4. DVD-Igs broadly recognize ebolavirus rVSV-GP particles in an FVM09-dependent manner. (A–B) Viral particles were normalized for GP content by ELISA with an ebolavirus GP peptide-specific polyclonal antiserum (*41*), captured onto plates, and probed with FVM09~548 (A) and FVM09~MR72 (B) in an ELISA. DVD-Ig binding was FVM09-dependent, since only nonspecific binding to viral particles was observed with parent IgG MR72 (B). Averages ± SD for 3 technical replicates from a representative experiment are shown. Two independent experiments were performed.

figure S5

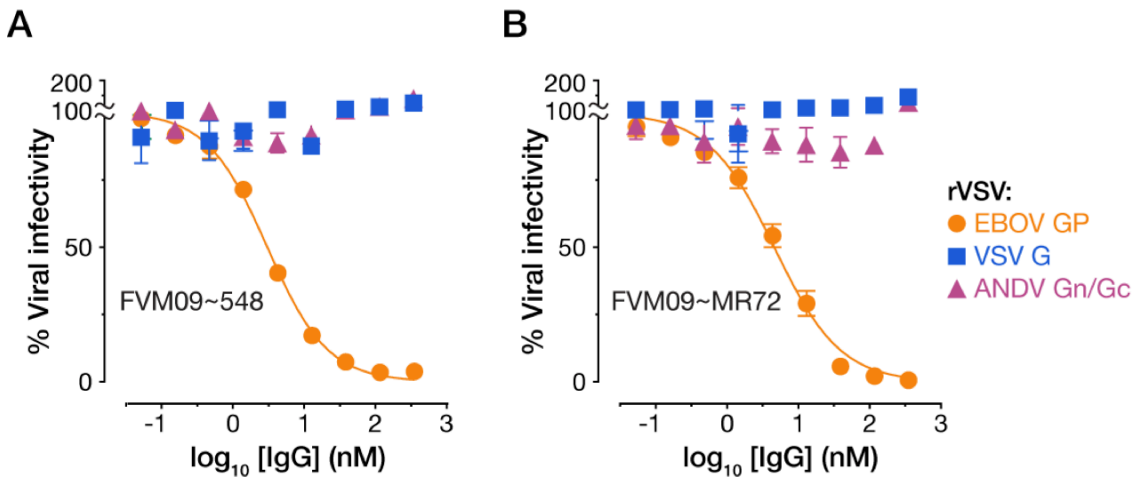

Figure S5. DVD-Igs specifically neutralize filovirus entry and infection. (A–B) Neutralization of rVSVs bearing EBOV GP or non-filovirus glycoproteins derived from a rhabdovirus (VSV G) and a hantavirus (Andes virus; ANDV Gn/Gc) by FVM09~548 (A) and FVM09~MR72 (B). Averages ± SD for 3 technical replicates from a representative experiment are shown. Two independent experiments were performed.

figure S6

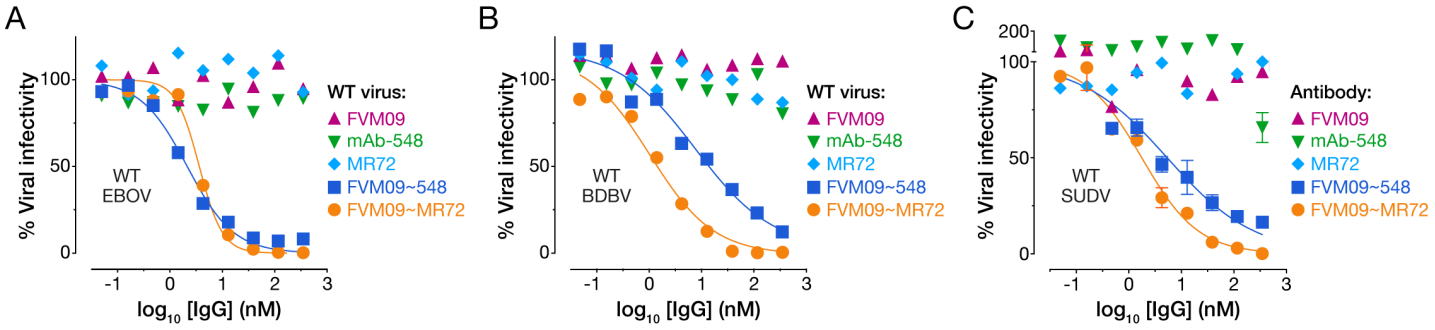

D

Antibody	rVSV-GP IC_{50} (nM)						WT virus IC_{50} (nM)		
	EBOV	BDBV	TAFV	SUDV	RESTV	MARV	EBOV	BDBV	SUDV
FVM09	>	nd	nd	>	nd	>	>	>	>
mAb-548	>	nd	nd	>	>	>	>	>	>
MR72	>	nd	nd	>	>	>	>	>	>
FVM09~548	2.9±0.2	1.3±0.1	3.0±0.3	60±10	12±3	>	2.1±0.4	8±3	5±2
FVM09~MR72	4.7±0.5	1.1±0.1	2.9±0.3	10±1	6±1	>	3.6±0.7	1.0±0.2	1.8±0.7

Figure S6. DVD-Igs, but not parent IgGs, possess broad neutralizing activity against authentic ebolaviruses. (A–C) Neutralization of authentic filoviruses in human U2OS osteosarcoma cells, measured in microneutralization assays. Infected cells were immunostained for viral antigen at 48 h post-infection, and enumerated by automated fluorescence microscopy. Averages ± SD (n=3) from 1–2 representative experiments are shown. (D) Ab concentrations at half-maximal neutralization (IC_{50} ± 95% confidence intervals for nonlinear curve fit of data in panels A–C) are shown. Averages ± SD for 4–6 technical replicates pooled from two independent experiments are shown.

figure S7

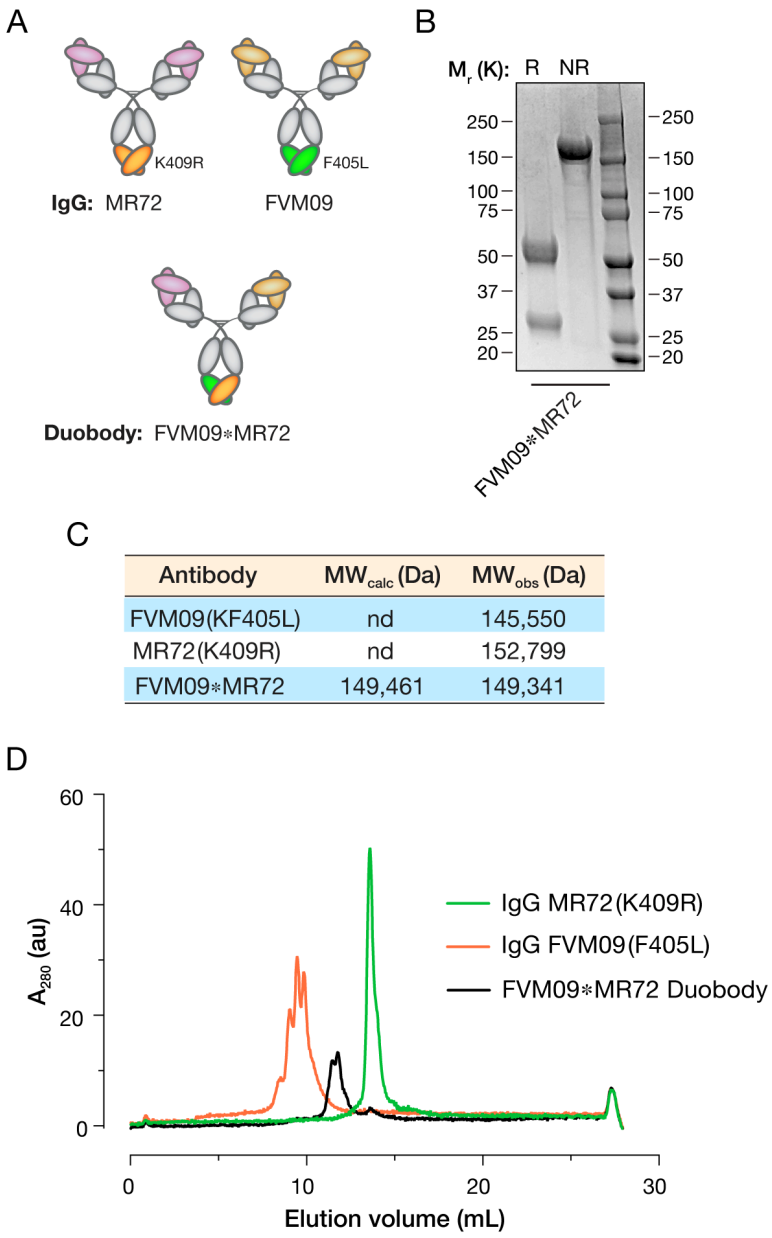

Antibody	MW_{calc} (Da)	MW_{obs} (Da)
FVM09(KF405L)	nd	145,550
MR72(K409R)	nd	152,799
FVM09∗MR72	149,461	149,341

Figure S7. DuoBody molecules combining extracellular 'delivery' and endosomal RBS-targeting specificities. (A) Schematic of MR72 (GP_{CL}-specific) and FVM09 (GP-specific) precursor mAbs (top row), and a DuoBody engineered to combine them (bottom row). The IgG CH3 mutations K409R and F405L promote heavy chain heterodimerization (*40*). (B) Biochemical characterization of IgGs and DuoBody. FVM09∗MR72 was resolved on SDS-polyacrylamide gels under reducing (R) and nonreducing (NR) conditions, and proteins were visualized by staining with Coomassie Brilliant Blue. (C) Parent IgGs and the post-exchange product (putative DuoBody) were analyzed by mass spectrometry (matrix-assisted laser desorption ionization-time of flight; MALDI-TOF). Calculated (MW_{calc}) and observed (MW_{obs}) molecular masses are indicated. nd, not determined. (D) Parent IgGs and post-exchange product (putative DuoBody) were analyzed by ion-exchange chromatography to determine the efficiency of Fab-arm exchange. The DuoBody eluted at a volume intermediate to those of the parent IgGs, and area-under-the-curve measurements indicated that the efficiency of exchange was ≈ 97%.

figure S8

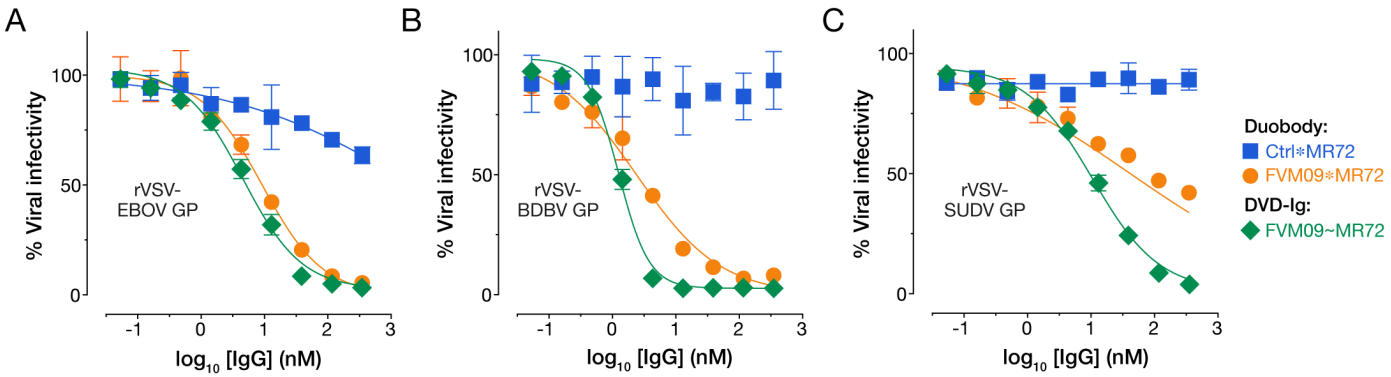

Figure S8. DuoBody combining FVM09 and MR72 possesses broad neutralizing activity. (A–C) Neutralizing activity of DuoBody molecules against rVSVs encoding eGFP and bearing ebolavirus GP proteins in human U2OS cells. See Fig. 2 for details. Averages ± SD (n=3) from a representative experiment are shown. Ctrl∗MR72 is a control DuoBody combining MR72 with an irrelevant IgG (HIV-1 specific IgG, b12). Averages ± SD for 4–6 technical replicates pooled from two independent experiments are shown.

figure S9

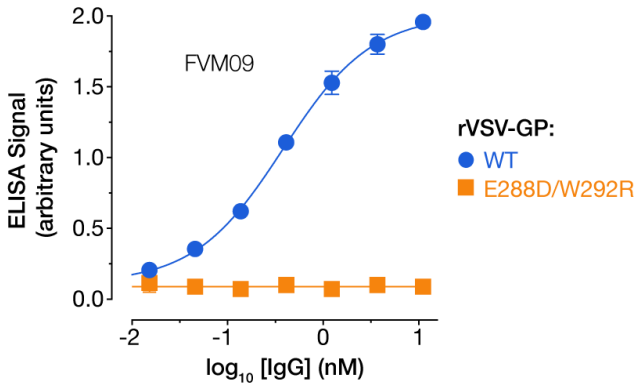

Figure S9. Two mutations in glycan cap subdomain of EBOV GP abolish FVM09 IgG binding. rVSV particles bearing EBOV GP(WT) or GP(E288D/W292R) were captured onto plates and probed with FVM09 IgG in an ELISA. Averages ± SD for 3 technical replicates from a representative experiment are shown. Two independent experiments were performed.

figure S10

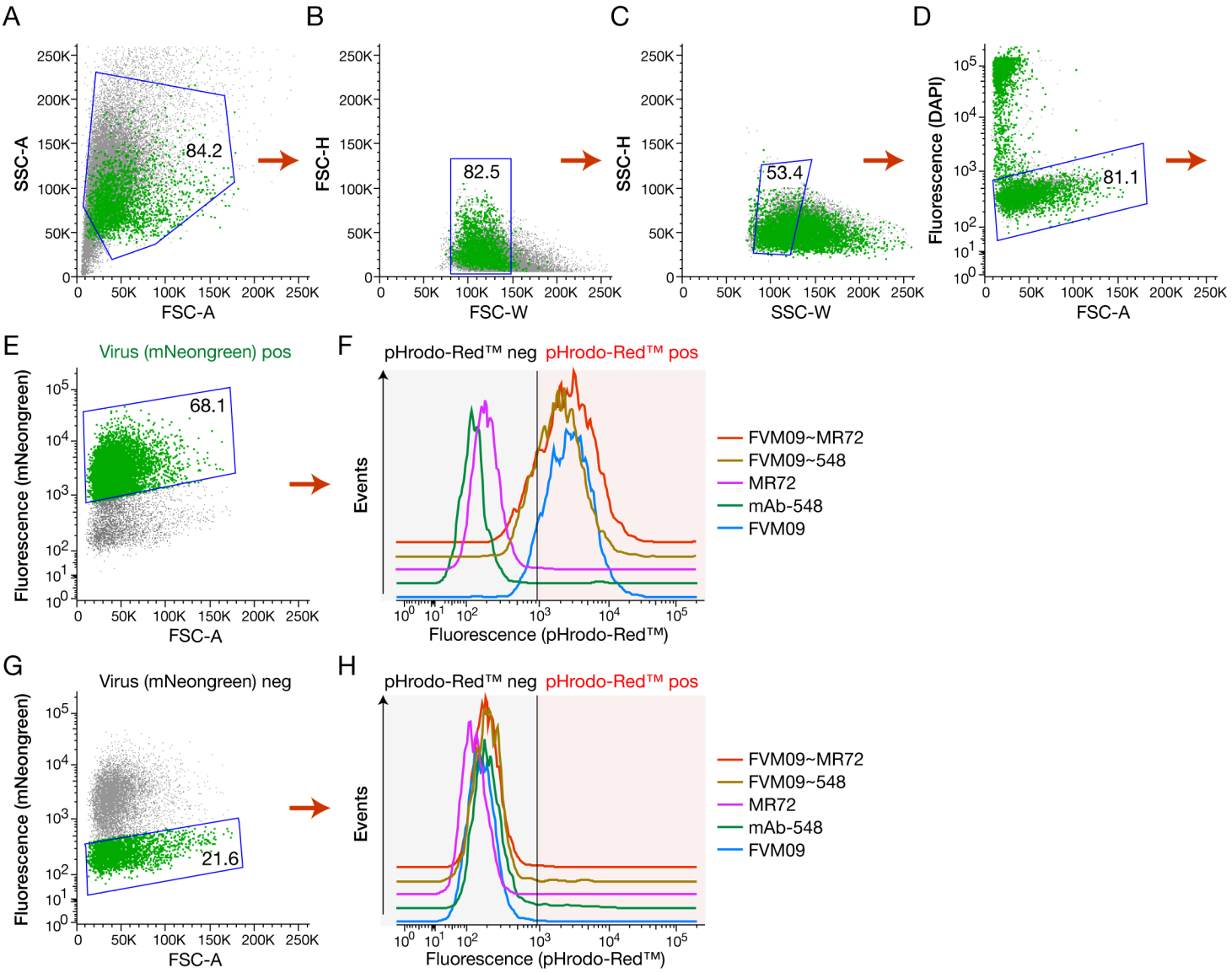

Figure S10. Workflow for flow cytometric measurement of Ab internalization into cells in the absence or presence of viral particles. Parent IgGs and DVD-Igs were covalently labeled with the acid-dependent fluorophore pHrodo Red™. Labeled Abs were incubated with rVSV-EBOV GP particles containing an internal fluorescent protein label (mNeongreen), and then exposed to U2OS cells for 30 min at 37˚C. Cells were chilled and then analyzed on a BD LSRII. Cells were first gated on side (A) and forward (B) scatter to gate out debris. Cells were then gated using pulse width/height (C) and nuclear DNA content (DAPI) (D) to identify a singlet population for further analysis. Virus^{+} (E) and virus^{-} (G) subpopulations were identified on the basis of mNeongreen fluorescence, and each was separately analyzed for pHrodo Red fluorescence (F–H).

figure S11

A

Two-way ANOVA	Sum of squares	df	Mean square	F (DFn, DFd)	Significance (*p*)
pHrodo-Red-labeled Ab	22483	5	4497	F (5, 36) = 319.5	<0.0001
mNeongreen-labeled rVSV-GP	25858	1	25858	F (1, 36) = 1837	<0.0001
Interaction (Ab x virus)	21998	5	4400	F (5, 36) = 312.6	<0.0001
Residual	507	36	14		

B

Multiple comparisons (Šídák's *post hoc* test)
(% Ab-positive cells, virus-negative cells vs. virus-positive cells)

pHrodo-Red-labeled Ab	Mean difference	95% CI of diff.	Significance (*p*)
No Ab control	0	-7 to 7	ns
FVM09	-91.6	-98.9 to -84.2	<0.0001
mAb-548	-6.27	-13.7 to 1.11	ns
MR72	-4.69	-12.1 to 2.69	ns
FVM09~548	-86.1	-93.5 to -78.7	<0.0001
FVM09~MR72	-89.8	-97.2 to -82.4	<0.0001

C

Multiple comparisons (Dunnett's *post hoc* test)
(% Ab-positive cells, 'no Ab' control vs. test Ab in virus-negative cells)

pHrodo-Red-labeled Ab	Mean difference	95% CI of diff.	Significance (*p*)
No Ab vs. FVM09	-1	-8 to 6	ns
No Ab vs. mAb-548	-1	-8 to 6	ns
No Ab vs. MR72	0	-7 to 7	ns
No Ab vs. FVM09~548	-1	-8 to 6	ns
No Ab vs. FVM09~MR72	0	-7 to 7	ns

D

Multiple comparisons (Dunnett's *post hoc* test)
(% Ab-positive cells, 'no Ab' control vs. test Ab in virus-positive cells)

pHrodo-Red-labeled Ab	Mean difference	95% CI of diff.	Significance (*p*)
No Ab vs. FVM09	-93	-99 to -85	<0.0001
No Ab vs. mAb-548	-7	-14 to 0	ns
No Ab vs. MR72	-5	-11 to 2	ns
No Ab vs. FVM09~548	-87	-94 to -80	<0.0001
No Ab vs. FVM09~MR72	-90	-97 to -83	<0.0001

Figure S11. Statistical analysis of Ab internalization into cells (Figs. 3D & S10). Results from the flow cytometric measurement of Ab internalization into cells in Figs. 3D and S10 were subjected to a two-way analysis of variance (ANOVA). (A) The influence of two independent variables (presence or absence of mNeongreen-labeled rVSV-EBOV GP particles, identity of pHrodo Red-labeled Ab) on the dependent variable (%Ab$^+$ cells) was determined. Ab internalization was significantly higher in virus$^+$ than in virus$^-$ cells, and was significantly dependent on both Ab identity, and on the interaction between virus and Ab. df, degrees of freedom. (B) Šídák's *post hoc* test was used to compare %Ab$^+$ cells in virus$^-$ vs. virus$^+$ cells, for each test Ab. (C–D) Dunnett's *post hoc* test was used to compare %Ab$^+$ cells obtained for each test Ab vs. the 'no Ab' control in virus$^-$ (C) and virus$^+$ (D) cell populations.

figure S12

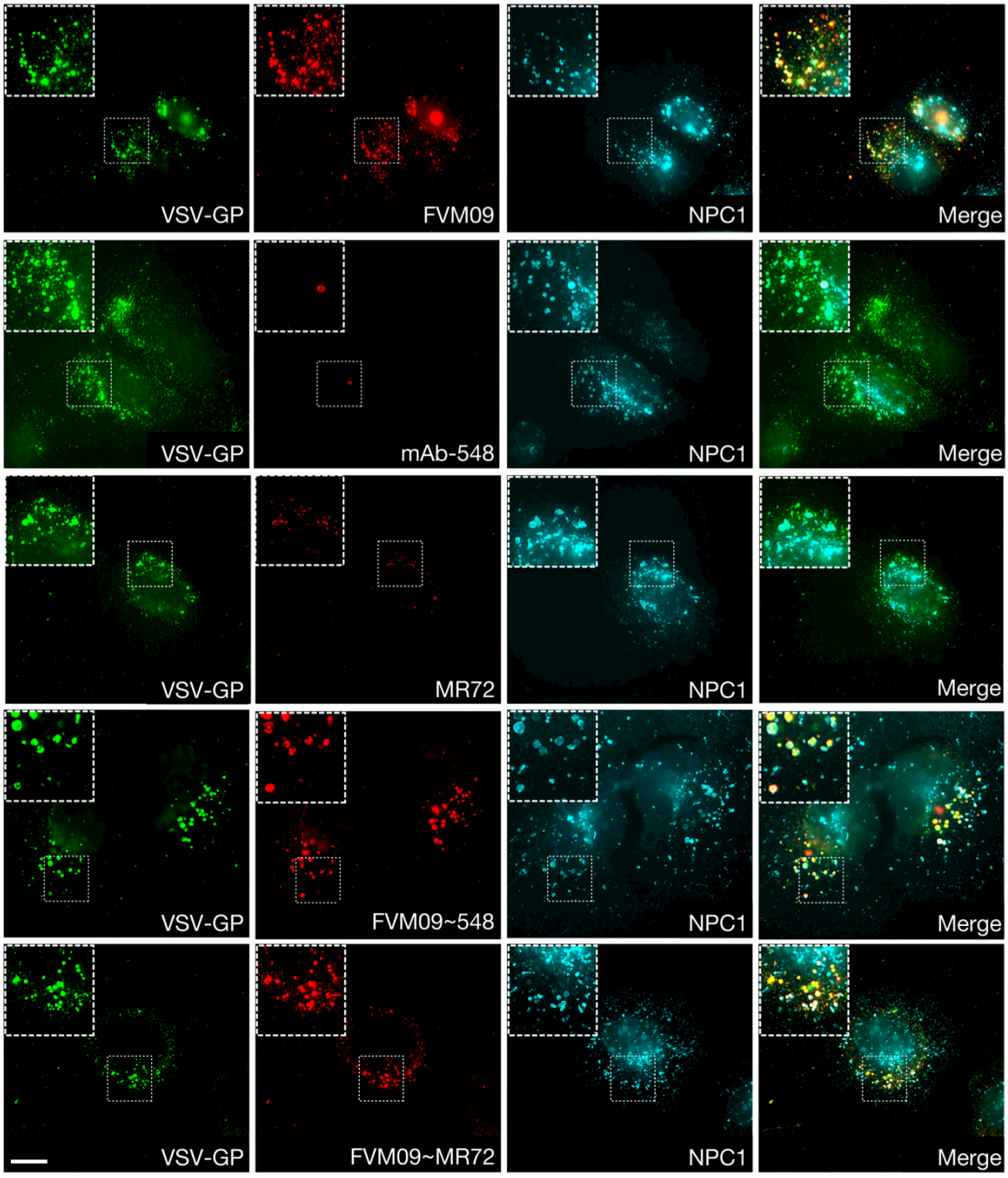

Figure S12. DVD-Igs, but not parent IgGs, undergo virion- and FVM09-dependent delivery to NPC1^{+} cellular compartments. Parent IgGs and DVD-Igs were incubated with mNeongreen-labeled rVSV-EBOV GP particles and then exposed to U2OS cells expressing an NPC1-enhanced blue fluorescent protein-2 fusion protein for 60 min at 37˚C. Cells were fixed, permeabilized, and immunostained, and viral particles, Ab, and NPC1 were visualized by fluorescence microscopy. Images from a representative experiment are shown. At least two independent experiments were performed. Scale bar, 20 μm.

figure S13

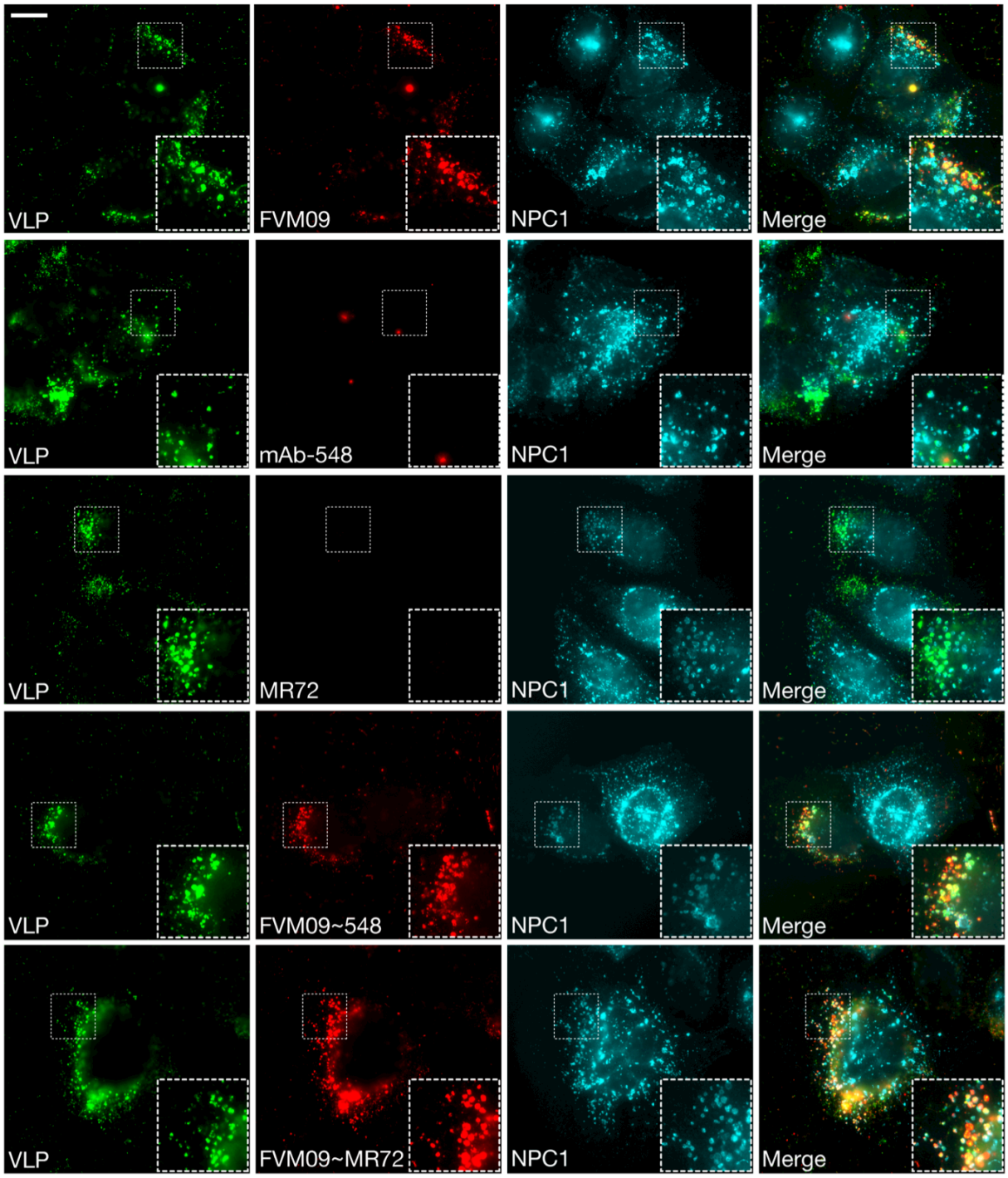

Figure S13. DVD-Igs, but not parent IgGs, undergo EBOV VLP- and FVM09-dependent delivery to $NPC1^{+}$ cellular compartments. Parent IgGs and DVD-Igs were incubated with EBOV GP/VP40 VLPs, and then exposed to U2OS cells expressing an NPC1-enhanced blue fluorescent protein-2 fusion protein for 60 min at 37˚C. Cells were fixed, permeabilized, and immunostained, and VLPs, Ab, and NPC1 were visualized by fluorescence microscopy. Images from a representative experiment are shown. Two independent experiments were performed. Scale bar, 20 μm.

figure S14

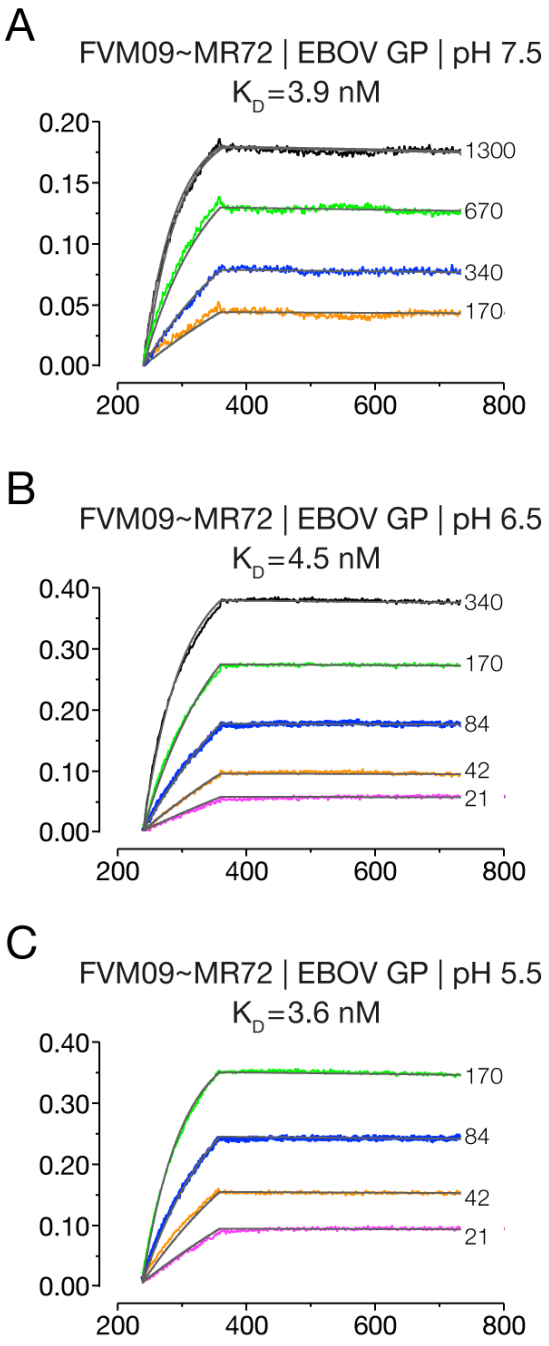

Figure S14. FVM09 bind to uncleaved EBOV GP with similar affinity at neutral pH and the presumptive acidic pH of early and late endosomes. Kinetic binding curves for FVM09~MR72 DVD-Ig:EBOV GP binding were determined by BLI at pH 7.5 (A), pH 6.5 (B), and pH 5.5 (C). FVM09~MR72 was loaded onto probes at pH 7.5, which were then equilibrated in buffer adjusted to the test pH, and dipped in analyte solutions. Gray lines show curve fits to a 1:1 binding model. See table S1 for kinetic binding constants. Representative data from two independent experiments are shown.

figure S15

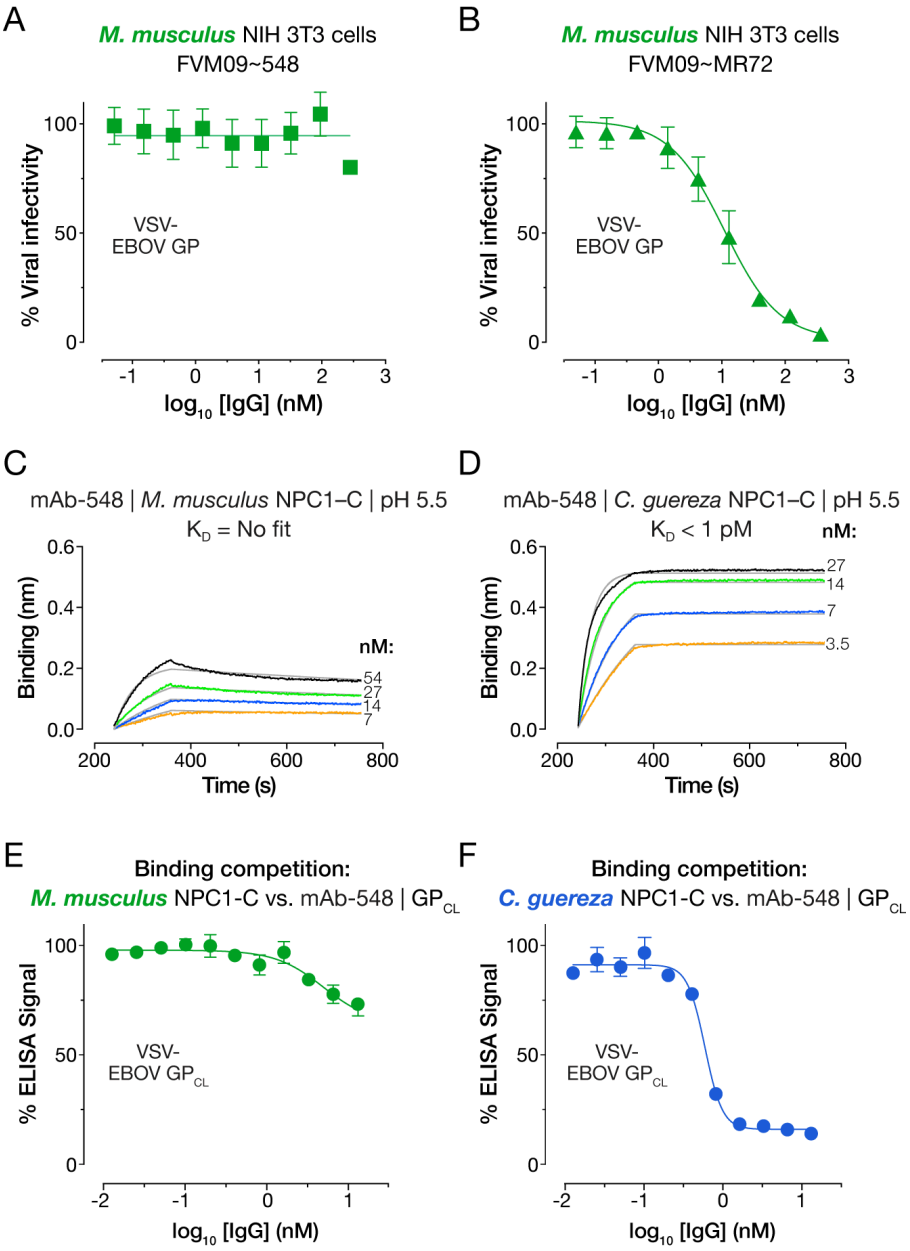

Figure S15. FVM09~548 lacks neutralizing activity in murine cells, because it binds weakly to the murine (*M. musculus*) NPC1 ortholog and only poorly blocks GP_{CL}-NPC1 interaction. (A–B) Neutralization of rVSV-EBOV GP infection in murine NIH/3T3 cells by the FVM09~548 and FVM09~MR72 DVD-Igs. (C–D) Kinetic binding curves for FVM09~548:NPC1–C interaction were determined by BLI. FVM09~548 was loaded onto probes, which were dipped in (C) murine NPC1–C or (D) mantled guereza (*C. guereza*) non-human primate NPC1–C analyte solutions. (E–F) Dose-dependent inhibition of rVSV-EBOV GP_{CL}:NPC1–C binding by mAb-548 in a competition ELISA. (C) Murine NPC1–C. (D) Mantled guereza NPC1–C. Gray lines show curve fits to a 1:1 binding model. In panels A, B, E, F, averages ± SD for 3 technical replicates from a representative experiment are shown. At least 2 independent experiments were performed. In panels C-D, representative curves from 2 independent experiments are shown. See table S1 for kinetic binding constants.

figure S16

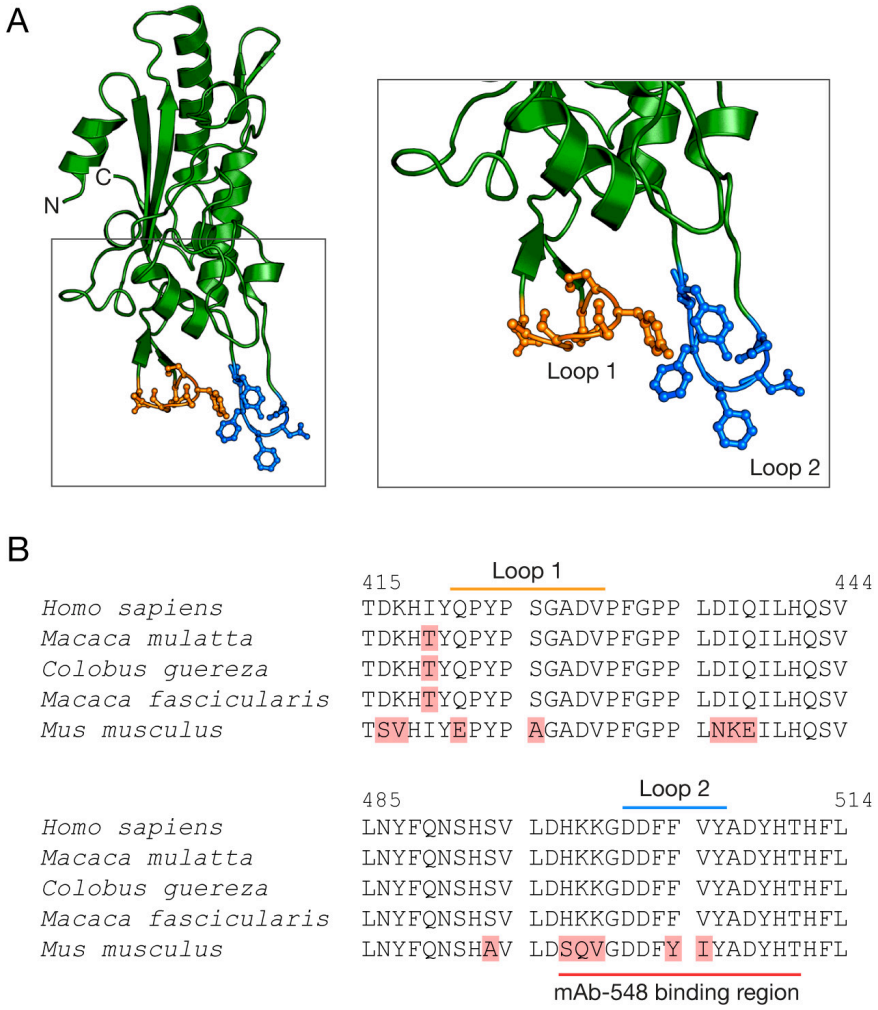

Figure S16. Amino acid sequence divergence of murine and primate NPC1 orthologs at the GP_{CL} binding interface. (A) Left, cartoon representation of human NPC1–C (PDB ID: 5F1B) (*16*). Boxed region is magnified at right, to highlight GP_{CL}-contacting loops 1 and 2 (balls and sticks). (B) Amino acid sequence alignments of NPC1–C sequences corresponding to loops 1 and 2, and the mAb-548-binding region. Sequence differences are highlighted.

table S1

Expt.	Antibody	Antigen	pH	k_{on} (M^{-1} s^{-1})[a]	k_{off} (s^{-1})[b]	K_D (nM)[c]
1	FVM09	EBOV GP	7.5	$(1.200\pm0.004)\times10^{4}$	$(5.5\pm0.1)\times10^{-5}$	4.5±0.1
2	mAb-548	Human NPC1–C	7.5	$(1.870\pm0.004)\times10^{5}$	$<1.0\times10^{-7}$	<0.001
3	mAb-548	Human NPC1–C	5.5	$(2.020\pm0.005)\times10^{5}$	$<1.0\times10^{-7}$	<0.001
4	mAb-548	NHP[d] NPC1–C	5.5	$(2.24\pm0.01)\times10^{5}$	$<1.0\times10^{-7}$	<0.001
5	mAb-548	Mouse NPC1–C	5.5	No fit[e]	No fit	No fit
6	MR72	EBOV GP_{CL}	7.5	$(3.330\pm0.002)\times10^{6}$	$<1.0\times10^{-7}$	<0.001
7	FVM09~548	EBOV GP	7.5	$(1.220\pm0.004)\times10^{4}$	$(2.2\pm0.2)\times10^{-5}$	1.8±0.1
8	FVM09~548	Human NPC1–C	7.5	$(8.58\pm0.08)\times10^{4}$	$<1.0\times10^{-7}$	<0.001
9	FVM09~MR72	EBOV GP	7.5	$(1.45\pm0.02)\times10^{4}$	$(5.8\pm0.2)\times10^{-5}$	3.9±0.2
10	FVM09~MR72	EBOV GP	6.5	$(4.97\pm0.02)\times10^{6}$	$(2.2\pm0.1)\times10^{-4}$	4.5±0.3
11	FVM09~MR72	EBOV GP	5.5	$(0.98\pm0.04)\times10^{6}$	$(3.5\pm0.2)\times10^{-4}$	3.6±0.2
12	FVM09~MR72	EBOV GP_{CL}	7.5	$(3.55\pm0.03)\times10^{6}$	$(1.98\pm0.03)\times10^{-4}$	0.055±0.001

Table S1. Kinetic binding constants for Ab:antigen interaction determined by BLI and fitting to a 1:1 binding model. Value ± 95% confidence intervals, determined from a representative experiment, are shown for each constant. At least two independent experiments were performed for each binding interaction.
(a) k_{on}, association rate constant
(b) k_{off}, dissociation rate constant
(c) K_D, equilibrium dissociation constant
(d) Mantled guereza NPC1–C (see figs. S15 & S16)
(e) Fits to 1:1 binding model did not converge.

References and Notes

1. X. Qiu, G. Wong, J. Audet, A. Bello, L. Fernando, J. B. Alimonti, H. Fausther-Bovendo, H. Wei, J. Aviles, E. Hiatt, A. Johnson, J. Morton, K. Swope, O. Bohorov, N. Bohorova, C. Goodman, D. Kim, M. H. Pauly, J. Velasco, J. Pettitt, G. G. Olinger, K. Whaley, B. Xu, J. E. Strong, L. Zeitlin, G. P. Kobinger, Reversion of advanced Ebola virus disease in nonhuman primates with ZMapp. *Nature* **514**, 47–53 (2014). Medline

2. C. D. Murin, M. L. Fusco, Z. A. Bornholdt, X. Qiu, G. G. Olinger, L. Zeitlin, G. P. Kobinger, A. B. Ward, E. O. Saphire, Structures of protective antibodies reveal sites of vulnerability on Ebola virus. *Proc. Natl. Acad. Sci. U.S.A.* **111**, 17182–17187 (2014). Medline doi:10.1073/pnas.1414164111

3. K. A. Howell, X. Qiu, J. M. Brannan, C. Bryan, E. Davidson, F. W. Holtsberg, A. Z. Wec, S. Shulenin, J. E. Biggins, R. Douglas, S. G. Enterlein, H. L. Turner, J. Pallesen, C. D. Murin, S. He, A. Kroeker, H. Vu, A. S. Herbert, M. L. Fusco, E. K. Nyakatura, J. R. Lai, Z. Y. Keck, S. K. Foung, E. O. Saphire, L. Zeitlin, A. B. Ward, K. Chandran, B. J. Doranz, G. P. Kobinger, J. M. Dye, M. J. Aman, Antibody treatment of Ebola and Sudan virus infection via a uniquely exposed epitope within the glycoprotein receptor-binding site. *Cell Rep.* **15**, 1514–1526 (2016). Medline doi:10.1016/j.celrep.2016.04.026

4. A. I. Flyak, X. Shen, C. D. Murin, H. L. Turner, J. A. David, M. L. Fusco, R. Lampley, N. Kose, P. A. Ilinykh, N. Kuzmina, A. Branchizio, H. King, L. Brown, C. Bryan, E. Davidson, B. J. Doranz, J. C. Slaughter, G. Sapparapu, C. Klages, T. G. Ksiazek, E. O. Saphire, A. B. Ward, A. Bukreyev, J. E. Crowe Jr., Cross-reactive and potent neutralizing antibody responses in human survivors of natural ebolavirus infection. *Cell* **164**, 392–405 (2016). Medline doi:10.1016/j.cell.2015.12.022

5. J. C. Frei, E. K. Nyakatura, S. E. Zak, R. R. Bakken, K. Chandran, J. M. Dye, J. R. Lai, Bispecific antibody affords complete post-exposure protection of mice from both Ebola (Zaire) and Sudan viruses. *Sci Rep* **6**, 19193 (2016). Medline doi:10.1038/srep19193

6. W. Furuyama, A. Marzi, A. Nanbo, E. Haddock, J. Maruyama, H. Miyamoto, M. Igarashi, R. Yoshida, O. Noyori, H. Feldmann, A. Takada, Discovery of an antibody for pan-ebolavirus therapy. *Sci Rep* **6**, 20514 (2016). Medline doi:10.1038/srep20514

7. F. W. Holtsberg, S. Shulenin, H. Vu, K. A. Howell, S. J. Patel, B. Gunn, M. Karim, J. R. Lai, J. C. Frei, E. K. Nyakatura, L. Zeitlin, R. Douglas, M. L. Fusco, J. W. Froude, E. O. Saphire, A. S. Herbert, A. S. Wirchnianski, C. M. Lear-Rooney, G. Alter, J. M. Dye, P. J. Glass, K. L. Warfield, M. J. Aman, Pan-ebolavirus and pan-filovirus mouse monoclonal antibodies: protection against Ebola and Sudan viruses. *J. Virol.* **90**, 266–278 (2016). Medline doi:10.1128/JVI.02171-15

8. Z. Y. Keck, S. G. Enterlein, K. A. Howell, H. Vu, S. Shulenin, K. L. Warfield, J. W. Froude, N. Araghi, R. Douglas, J. Biggins, C. M. Lear-Rooney, A. S. Wirchnianski, P. Lau, Y. Wang, A. S. Herbert, J. M. Dye, P. J. Glass, F. W. Holtsberg, S. K. Foung, M. J. Aman, Macaque monoclonal antibodies targeting novel conserved epitopes within filovirus glycoprotein. *J. Virol.* **90**, 279–291 (2016). Medline doi:10.1128/JVI.02172-15

9. K. Chandran, N. J. Sullivan, U. Felbor, S. P. Whelan, J. M. Cunningham, Endosomal proteolysis of the Ebola virus glycoprotein is necessary for infection. *Science* **308**, 1643–1645 (2005). Medline doi:10.1126/science.1110656

10. K. Schornberg, S. Matsuyama, K. Kabsch, S. Delos, A. Bouton, J. White, Role of endosomal cathepsins in entry mediated by the Ebola virus glycoprotein. *J. Virol.* **80**, 4174–4178 (2006). Medline doi:10.1128/JVI.80.8.4174-4178.2006

11. E. H. Miller, G. Obernosterer, M. Raaben, A. S. Herbert, M. S. Deffieu, A. Krishnan, E. Ndungo, R. G. Sandesara, J. E. Carette, A. I. Kuehne, G. Ruthel, S. R. Pfeffer, J. M. Dye, S. P. Whelan, T. R. Brummelkamp, K. Chandran, Ebola virus entry requires the host-programmed recognition of an intracellular receptor. *EMBO J.* **31**, 1947–1960 (2012). Medline doi:10.1038/emboj.2012.53

12. J. E. Carette, M. Raaben, A. C. Wong, A. S. Herbert, G. Obernosterer, N. Mulherkar, A. I. Kuehne, P. J. Kranzusch, A. M. Griffin, G. Ruthel, P. Dal Cin, J. M. Dye, S. P. Whelan, K. Chandran, T. R. Brummelkamp, Ebola virus entry requires the cholesterol transporter Niemann-Pick C1. *Nature* **477**, 340–343 (2011). Medline doi:10.1038/nature10348

13. M. Côté, J. Misasi, T. Ren, A. Bruchez, K. Lee, C. M. Filone, L. Hensley, Q. Li, D. Ory, K. Chandran, J. Cunningham, Small molecule inhibitors reveal Niemann-Pick C1 is essential for Ebola virus infection. *Nature* **477**, 344–348 (2011). Medline doi:10.1038/nature10380

14. A. S. Herbert, C. Davidson, A. I. Kuehne, R. Bakken, S. Z. Braigen, K. E. Gunn, S. P. Whelan, T. R. Brummelkamp, N. A. Twenhafel, K. Chandran, S. U. Walkley, J. M. Dye, Niemann-pick C1 is essential for ebolavirus replication and pathogenesis in vivo. *MBio* **6**, e00565-e15 (2015). Medline doi:10.1128/mBio.00565-15

15. Z. A. Bornholdt, E. Ndungo, M. L. Fusco, S. Bale, A. I. Flyak, J. E. Crowe Jr., K. Chandran, E. O. Saphire, Host-primed Ebola virus GP exposes a hydrophobic NPC1 receptor-binding pocket, revealing a target for broadly neutralizing antibodies. *MBio* **7**, e02154-e15 (2016). Medline

16. H. Wang, Y. Shi, J. Song, J. Qi, G. Lu, J. Yan, G. F. Gao, Ebola viral glycoprotein bound to its endosomal receptor Niemann-Pick C1. *Cell* **164**, 258–268 (2016). Medline doi:10.1016/j.cell.2015.12.044

17. M. A. Brindley, L. Hughes, A. Ruiz, P. B. McCray Jr., A. Sanchez, D. A. Sanders, W. Maury, Ebola virus glycoprotein 1: Identification of residues important for binding and postbinding events. *J. Virol.* **81**, 7702–7709 (2007). Medline doi:10.1128/JVI.02433-06

18. B. Manicassamy, J. Wang, H. Jiang, L. Rong, Comprehensive analysis of Ebola virus GP1 in viral entry. *J. Virol.* **79**, 4793–4805 (2005). Medline doi:10.1128/JVI.79.8.4793-4805.2005

19. J. S. Spence, T. B. Krause, E. Mittler, R. K. Jangra, K. Chandran, Direct visualization of Ebola virus fusion triggering in the endocytic pathway. *MBio* **7**, e01857-e15 (2016). Medline doi:10.1128/mBio.01857-15

20. M. J. Aman, Chasing Ebola through the endosomal labyrinth. *MBio* **7**, e00346-e16 (2016). Medline doi:10.1128/mBio.00346-16

21. M. Ng, E. Ndungo, R. K. Jangra, Y. Cai, E. Postnikova, S. R. Radoshitzky, J. M. Dye, E. Ramírez de Arellano, A. Negredo, G. Palacios, J. H. Kuhn, K. Chandran, Cell entry by a novel European filovirus requires host endosomal cysteine proteases and Niemann-Pick C1. *Virology* **468-470**, 637–646 (2014). Medline doi:10.1016/j.virol.2014.08.019

22. T. Hashiguchi, M. L. Fusco, Z. A. Bornholdt, J. E. Lee, A. I. Flyak, R. Matsuoka, D. Kohda, Y. Yanagi, M. Hammel, J. E. Crowe Jr., E. O. Saphire, Structural basis for Marburg virus neutralization by a cross-reactive human antibody. *Cell* **160**, 904–912 (2015). Medline doi:10.1016/j.cell.2015.01.041

23. A. I. Flyak, P. A. Ilinykh, C. D. Murin, T. Garron, X. Shen, M. L. Fusco, T. Hashiguchi, Z. A. Bornholdt, J. C. Slaughter, G. Sapparapu, C. Klages, T. G. Ksiazek, A. B. Ward, E. O. Saphire, A. Bukreyev, J. E. Crowe Jr., Mechanism of human antibody-mediated neutralization of Marburg virus. *Cell* **160**, 893–903 (2015). Medline doi:10.1016/j.cell.2015.01.031

24. J. P. Davies, Y. A. Ioannou, Topological analysis of Niemann-Pick C1 protein reveals that the membrane orientation of the putative sterol-sensing domain is identical to those of 3-hydroxy-3-methylglutaryl-CoA reductase and sterol regulatory element binding protein cleavage-activating protein. *J. Biol. Chem.* **275**, 24367–24374 (2000). Medline doi:10.1074/jbc.M002184200

25. C. Wu, H. Ying, C. Grinnell, S. Bryant, R. Miller, A. Clabbers, S. Bose, D. McCarthy, R. R. Zhu, L. Santora, R. Davis-Taber, Y. Kunes, E. Fung, A. Schwartz, P. Sakorafas, J. Gu, E. Tarcsa, A. Murtaza, T. Ghayur, Simultaneous targeting of multiple disease mediators by a dual-variable-domain immunoglobulin. *Nat. Biotechnol.* **25**, 1290–1297 (2007). Medline doi:10.1038/nbt1345

26. L. M. Kleinfelter, R. K. Jangra, L. T. Jae, A. S. Herbert, E. Mittler, K. M. Stiles, A. S. Wirchnianski, M. Kielian, T. R. Brummelkamp, J. M. Dye, K. Chandran, Haploid genetic screen reveals a profound

and direct dependence on cholesterol for hantavirus membrane fusion. *MBio* **6**, e00801-15 (2015). Medline doi:10.1128/mBio.00801-15

27. M. Ng, E. Ndungo, M. E. Kaczmarek, A. S. Herbert, T. Binger, A. I. Kuehne, R. K. Jangra, J. A. Hawkins, R. J. Gifford, R. Biswas, A. Demogines, R. M. James, M. Yu, T. R. Brummelkamp, C. Drosten, L. F. Wang, J. H. Kuhn, M. A. Müller, J. M. Dye, S. L. Sawyer, K. Chandran, Filovirus receptor NPC1 contributes to species-specific patterns of ebolavirus susceptibility in bats. *Elife* **4**, e11785 (2015). Medline doi:10.7554/eLife.11785

28. E. Ndungo, A. S. Herbert, M. Raaben, G. Obernosterer, R. Biswas, E. H. Miller, A. S. Wirchnianski, J. E. Carette, T. R. Brummelkamp, S. P. Whelan, J. M. Dye, K. Chandran, A single residue in Ebola virus receptor NPC1 influences cellular host range in reptiles. *mSphere* **1**, e00007-16 (2016). Medline doi:10.1128/mSphere.00007-16

29. C. Spiess, Q. Zhai, P. J. Carter, Alternative molecular formats and therapeutic applications for bispecific antibodies. *Mol. Immunol.* **67** (2 Pt A), 95–106 (2015). Medline doi:10.1016/j.molimm.2015.01.003

30. A. F. Labrijn, J. I. Meesters, B. E. de Goeij, E. T. van den Bremer, J. Neijssen, M. D. van Kampen, K. Strumane, S. Verploegen, A. Kundu, M. J. Gramer, P. H. van Berkel, J. G. van de Winkel, J. Schuurman, P. W. Parren, Efficient generation of stable bispecific IgG1 by controlled Fab-arm exchange. *Proc. Natl. Acad. Sci. U.S.A.* **110**, 5145–5150 (2013). Medline doi:10.1073/pnas.1220145110

31. J. A. Simmons, R. S. D'Souza, M. Ruas, A. Galione, J. E. Casanova, J. M. White, Ebolavirus glycoprotein directs fusion through NPC1+ endolysosomes. *J. Virol.* **90**, 605–610 (2016). Medline doi:10.1128/JVI.01828-15

32. M. Bray, K. Davis, T. Geisbert, C. Schmaljohn, J. Huggins, A mouse model for evaluation of prophylaxis and therapy of Ebola hemorrhagic fever. *J. Infect. Dis.* **178**, 651–661 (1998). Medline doi:10.1086/515386

33. J. M. Brannan, J. W. Froude, L. I. Prugar, R. R. Bakken, S. E. Zak, S. P. Daye, C. E. Wilhelmsen, J. M. Dye, Interferon α/β receptor-deficient mice as a model for Ebola virus disease. *J. Infect. Dis.* **212** (Suppl 2), S282–S294 (2015). Medline doi:10.1093/infdis/jiv215

34. Z. A. Bornholdt, H. L. Turner, C. D. Murin, W. Li, D. Sok, C. A. Souders, A. E. Piper, A. Goff, J. D. Shamblin, S. E. Wollen, T. R. Sprague, M. L. Fusco, K. B. Pommert, L. A. Cavacini, H. L. Smith, M. Klempner, K. A. Reimann, E. Krauland, T. U. Gerngross, K. D. Wittrup, E. O. Saphire, D. R. Burton, P. J. Glass, A. B. Ward, L. M. Walker, Isolation of potent neutralizing antibodies from a survivor of the 2014 Ebola virus outbreak. *Science* **351**, 1078–1083 (2016). Medline doi:10.1126/science.aad5788

35. L. T. Jae, M. Raaben, A. S. Herbert, A. I. Kuehne, A. S. Wirchnianski, T. K. Soh, S. H. Stubbs, H. Janssen, M. Damme, P. Saftig, S. P. Whelan, J. M. Dye, T. R. Brummelkamp, Lassa virus entry requires a trigger-induced receptor switch. *Science* **344**, 1506–1510 (2014). Medline doi:10.1126/science.1252480

36. H. W. Ai, N. C. Shaner, Z. Cheng, R. Y. Tsien, R. E. Campbell, Exploration of new chromophore structures leads to the identification of improved blue fluorescent proteins. *Biochemistry* **46**, 5904–5910 (2007). Medline doi:10.1021/bi700199g

37. J. Sroubek, Y. Krishnan, J. Chinai, S. Buhl, M. D. Scharff, T. V. McDonald, The use of Bcl-2 over-expression to stabilize hybridomas specific to the HERG potassium channel. *J. Immunol. Methods* **375**, 215–222 (2012). Medline doi:10.1016/j.jim.2011.10.014

38. J. Ye, N. Ma, T. L. Madden, J. M. Ostell, IgBLAST: An immunoglobulin variable domain sequence analysis tool. *Nucleic Acids Res.* **41** (W1), W34–W40 (2013). Medline doi:10.1093/nar/gkt382

39. Y. Mazor, I. Barnea, I. Keydar, I. Benhar, Antibody internalization studied using a novel IgG binding toxin fusion. *J. Immunol. Methods* **321**, 41–59 (2007). Medline doi:10.1016/j.jim.2007.01.008

40. A. F. Labrijn, J. I. Meesters, P. Priem, R. N. de Jong, E. T. van den Bremer, M. D. van Kampen, A. F. Gerritsen, J. Schuurman, P. W. Parren, Controlled Fab-arm exchange for the generation of stable bispecific IgG1. *Nat. Protoc.* **9**, 2450–2463 (2014). Medline doi:10.1038/nprot.2014.169

41. J. Misasi, K. Chandran, J. Y. Yang, B. Considine, C. M. Filone, M. Côté, N. Sullivan, G. Fabozzi, L. Hensley, J. Cunningham, Filoviruses require endosomal cysteine proteases for entry but exhibit distinct protease preferences. *J. Virol.* **86**, 3284–3292 (2012). Medline doi:10.1128/JVI.06346-11

42. A. C. Wong, R. G. Sandesara, N. Mulherkar, S. P. Whelan, K. Chandran, A forward genetic strategy reveals destabilizing mutations in the ebolavirus glycoprotein that alter its protease dependence during cell entry. *J. Virol.* **84**, 163–175 (2010). Medline doi:10.1128/JVI.01832-09

43. D. H. Schott, D. K. Cureton, S. P. Whelan, C. P. Hunter, An antiviral role for the RNA interference machinery in *Caenorhabditis elegans*. *Proc. Natl. Acad. Sci. U.S.A.* **102**, 18420–18424 (2005). Medline doi:10.1073/pnas.0507123102

44. P. B. Jahrling, T. W. Geisbert, J. B. Geisbert, J. R. Swearengen, M. Bray, N. K. Jaax, J. W. Huggins, J. W. LeDuc, C. J. Peters, Evaluation of immune globulin and recombinant interferon-alpha2b for treatment of experimental Ebola virus infections. *J. Infect. Dis.* **179** (Suppl 1), S224–S234 (1999). Medline doi:10.1086/514310

45. Ebola haemorrhagic fever in Sudan, 1976. Report of a WHO/International Study Team. *Bull. World Health Organ.* **56**, 247–270 (1978). Medline

46. J. S. Towner, T. K. Sealy, M. L. Khristova, C. G. Albariño, S. Conlan, S. A. Reeder, P. L. Quan, W. I. Lipkin, R. Downing, J. W. Tappero, S. Okware, J. Lutwama, B. Bakamutumaho, J. Kayiwa, J. A. Comer, P. E. Rollin, T. G. Ksiazek, S. T. Nichol, Newly discovered ebola virus associated with hemorrhagic fever outbreak in Uganda. *PLOS Pathog.* **4**, e1000212 (2008). Medline doi:10.1371/journal.ppat.1000212

47. T. Maruyama, L. L. Rodriguez, P. B. Jahrling, A. Sanchez, A. S. Khan, S. T. Nichol, C. J. Peters, P. W. Parren, D. R. Burton, Ebola virus can be effectively neutralized by antibody produced in natural human infection. *J. Virol.* **73**, 6024–6030 (1999). Medline

48. K. L. Warfield, C. M. Bosio, B. C. Welcher, E. M. Deal, M. Mohamadzadeh, A. Schmaljohn, M. J. Aman, S. Bavari, Ebola virus-like particles protect from lethal Ebola virus infection. *Proc. Natl. Acad. Sci. U.S.A.* **100**, 15889–15894 (2003). Medline doi:10.1073/pnas.2237038100